ABSTRACT

Title of Document:	PROBING ALLOSTERIC COMMUNICATION BETWEEN DISORDERED SURFACES IN A PROTEIN
	William J. Cressman Master of Science, 2015
Directed By:	Dr. Dorothy Beckett Department of Chemistry and Biochemistry

Molecular mechanisms of protein allostery are not well understood, particularly in those systems that undergo disorder to order transitions upon activation. BirA is a model allosteric protein in which corepressor, bio-5'-AMP, binding enhances dimerization by -4 kcal/mol and is coupled to disordered loop folding on both functional surfaces. BirA variants with single alanine substitutions in dimerization surface residues are investigated to further characterize communication between the two sites. Isothermal titration calorimetry measurements of corepressor binding of these BirA variants indicate only the G142A substitution perturbs the free energy of binding. The G142A crystal structure indicates a mechanism of communication from the corepressor binding to the dimerization surface involving α-helical extension of residues 143-146. Measurements of heat capacity changes associated with corepressor binding to the BirA variants support a model in which the

helical extension enhances dimerization by enabling the formation of a network of

intramolecular interactions on the dimerization surface.

PROBING ALLOSTERIC COMMUNICATION BETWEEN DISORDERED
SURFACES IN A PROTEIN

By

William J. Cressman

Thesis submitted to the Faculty of the Graduate School of the
University of Maryland, College Park, in partial fulfillment
of the requirements for the degree of
Master of Biochemistry
2015

Advisory Committee:
Professor Dorothy Beckett, Chair
Professor Douglas Julin
Professor Nicole LaRonde

Dedication

For my father, Robert Cressman Jr., whose love of science could only be surpassed

by his passion for helping others.

Acknowledgements

Foremost, my advisor, Dr. Dorothy Beckett, whose efforts and guidance have made this thesis possible and made me the scientist I am today.

My wife, Stephanie, for her unwavering love and support.

My coworkers and friends, Chris Eginton and Jingheng Wang, who were a constant source of encouragement, suggestions and ideas.

My family and friends, for their unending support and encouragement.

Table of Contents

List of Tables

List of Figures

Chapter 1 : Introduction

Allostery in Protein Regulation

Allostery is defined as the functional regulation of one site on a protein by an effector at a second site. This effector could be any small ligand, macromolecule, or post-translational modification[1,2]. Biologically, allostery allows modulation of protein function based on environmental conditions and is therefore critical for regulation of numerous cellular processes including metabolism[3], transcription[4], and signal transduction[5].

Historically, the MWC[6] and KNF[7] allosteric models were developed to describe enzyme cooperativity. These models describe homotropic cooperativity using a 2-state, conformational change from a tense, T, to a relaxed, R, state. However, the molecular details of these T and R states could only be described when crystal structures, such as those first obtained for horse hemoglobin were obtained by Max Perutz in 1970[8]. With this data, he was able to develop a structural model for the T to R transition in hemoglobin. These structures allowed development of a molecular mechanism of the allosteric transition communication in hemoglobin in which O_2 binding induces the breakage of constraining inter-subunit salt bridges. When these intermolecular salt bridges are removed, the free energy of subsequent O_2 binding steps is more favorable leading to positive homotropic cooperativity.

Allosteric mechanisms for proteins have now been characterized for a number of other systems. For example, Datta et. al. observed a pathway of 21 hydrogen bonds connecting the allosterically activated site to the modified functional sites in the

caspase-1 dimer. Only 12 of these hydrogen bonds were present in the apo protein[9]. Alanine mutagenesis significantly alters protease activity for four residues spanning the distance between the two sites indicating an apparent allosteric pathway.

However, the secondary structure of proteins is not necessarily well defined. Both partially disordered proteins and intrinsically disorder proteins (IDPs) that have no well-defined secondary structure have been characterized[10,11]. Biologically, protein disorder is thought to allow for multispecificity in protein-protein interactions and is widely observed in signaling and regulatory pathways[12,13]. The folding of disordered regions upon effector binding allows the formation of additional intramolecular interactions associated with allosteric regulation. However, disorder to order transitions and their mechanistic roles in protein allostery are not well understood. Above 30% of all protein residues in eukaryotes are predicted to contain disordered regions[14] and this knowledge gap could prove to be a significant barrier to protein structure-function prediction and drug design. Within this thesis the allosteric mechanism in one model protein, BirA, for which disordered loop folding is coupled to its allosteric activation is investigated.

BirA as a model allosteric system

E. coli BirA functions as both a transcriptional repressor and critical enzyme for fatty acid biosynthesis (**Figure 1.1**). Both functions require BirA-catalyzed synthesis of its corepressor, bio-5'-AMP, from biotin and ATP. The corepressor remains tightly bound to BirA after synthesis, enhancing homodimerization by -4
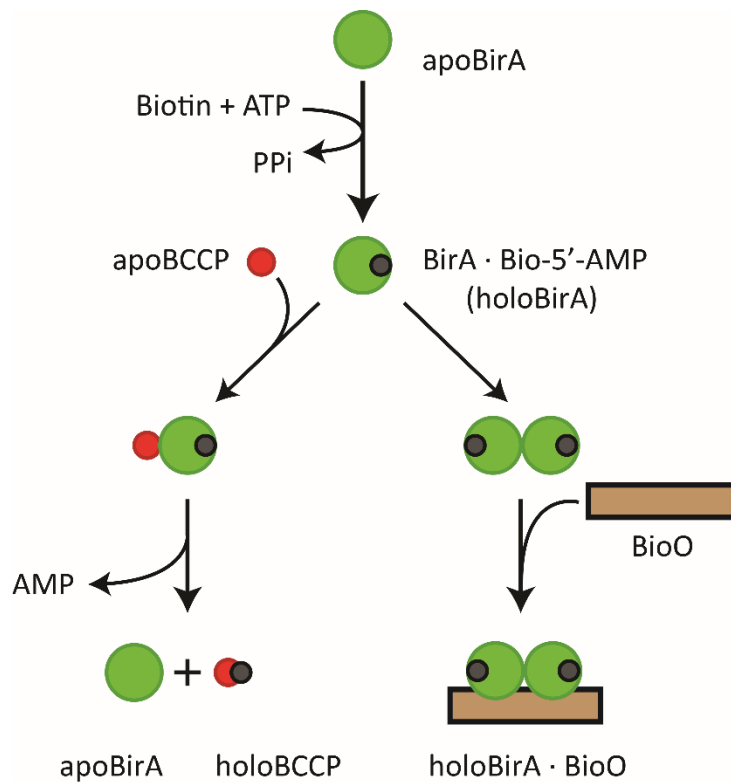
Figure 1.1: BirA in the E.coli biotin regulatory system.
Following bio-5'-AMP synthesis, holoBirA dimerizes to form either a catalytic heterodimer (left) or a DNA-binding homodimer (right) on the same dimerization surface[15].
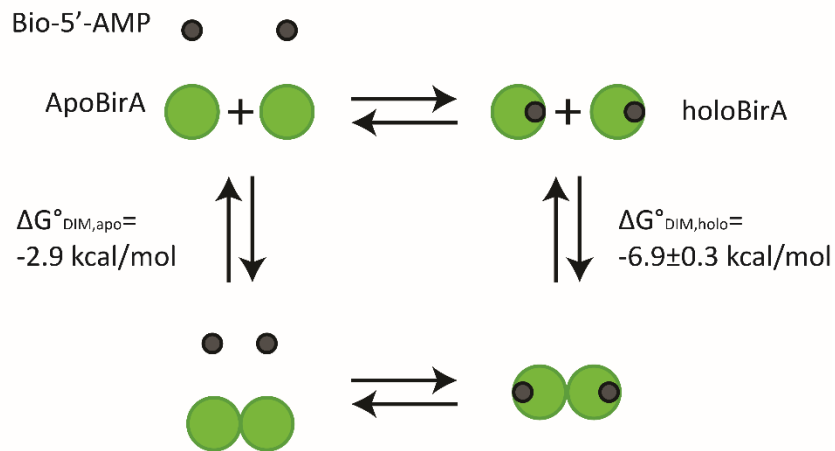
Coupling Free Energy
$$\Delta\Delta G°_{c,DIM}=\Delta G_{DIM,holo}-\Delta G_{DIM,apo}=-4.0\pm0.3 \text{ kcal/mol}$$

Figure 1.2: Thermodynamic cycle illustrating coupled bio-5'-AMP binding and dimerization.
Binding of corepressor bio-5'-AMP enhances dimerization by the coupling free energy, -4.0±0.3kcal/mol[16].

kcal/mol[17]. Following dimerization, BirA binds to the biotin operator, BioO,

repressing transcription of biotin biosynthetic genes[17]. Bio-5'-AMP binding and

subsequent homodimerization are important elements of the regulation of biotin

biosynthesis in *E. coli*. Moreover this process serves as a model system for studying

the mechanistic basis of protein allostery.

Disordered loops play a role in the BirA allosteric mechanism

Bio-5'AMP binding occurs at a site which includes two loops that are

unfolded prior to ligand binding. Residues 116-126, the biotin binding loop (BBL),

fold when biotin is bound. In addition to the BBL, residues 211-234, the adenylate

binding loop (ABL), become ordered upon bio-5'-AMP binding (**Figure 1.3**).

The ABL is critical for adenylate binding as evidenced by single alanine substitutions

in this loop, which perturb bio-5'-AMP binding by up to 3.4 kcal/mol[18]. Upon bio-5'-

AMP binding, a majority of these BirA variants also show decreased protein

protection from site-specific subtilisin cleavage between residues 217 and 218 in the

ABL, consistent with perturbation of loop folding[18,19]. Substitutions in the ABL also

perturb holoBirA dimerization free energy by 0.5-1.5 kcal/mol, indicating functional

communication to the dimerization surface. Together, these results are consistent with

communication from the ligand binding surface to the dimerization surface by

coupled corepressor binding and ABL folding.

Similarly, perturbations were made in several dimerization surface loops to

investigate their role in assembly of the BirA dimer. Alanine substitutions were made

in four dimerization surface loops comprised of residues 140-143, 170-167, 193-197,

and 280-283. These substitutions are all located in the dimerization interface

4
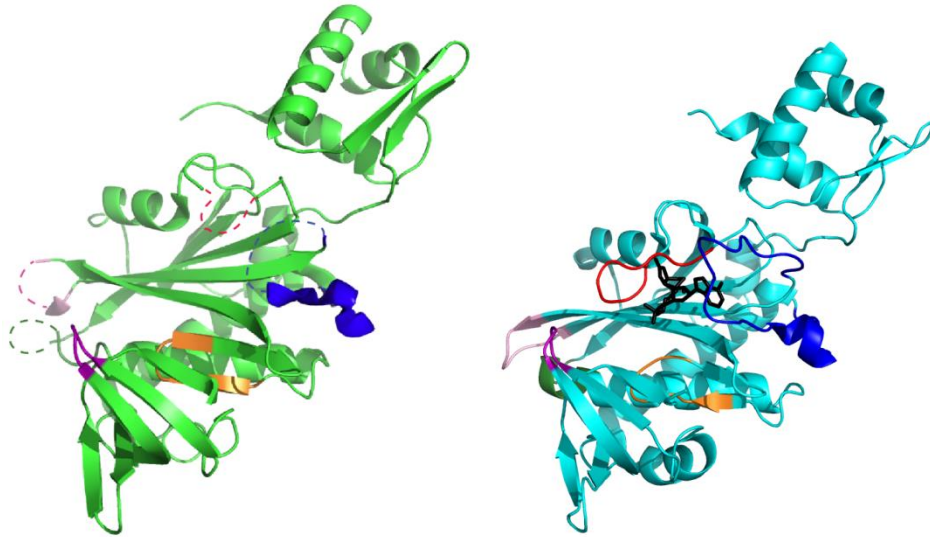
Figure 1.3: Structural comparison of apo and holoBirA.
Apo BirA (PDB entry 1BIA) and a monomer of the holoBirA dimer (PDB entry 2EWN) are shown with the non-hydrolysable bio-5'-AMP analog, biotinol-5'-AMP (black), bound. Following ligand binding and subsequent dimerization, residues 116-124 (red), 212-222 (blue), and 194-197 (pink), and glycine 142 of the 140-143 (dark green) loops become ordered. Residues in the 170-176 (orange) and 280-283 (purple) loops are folded regardless of ligand binding.
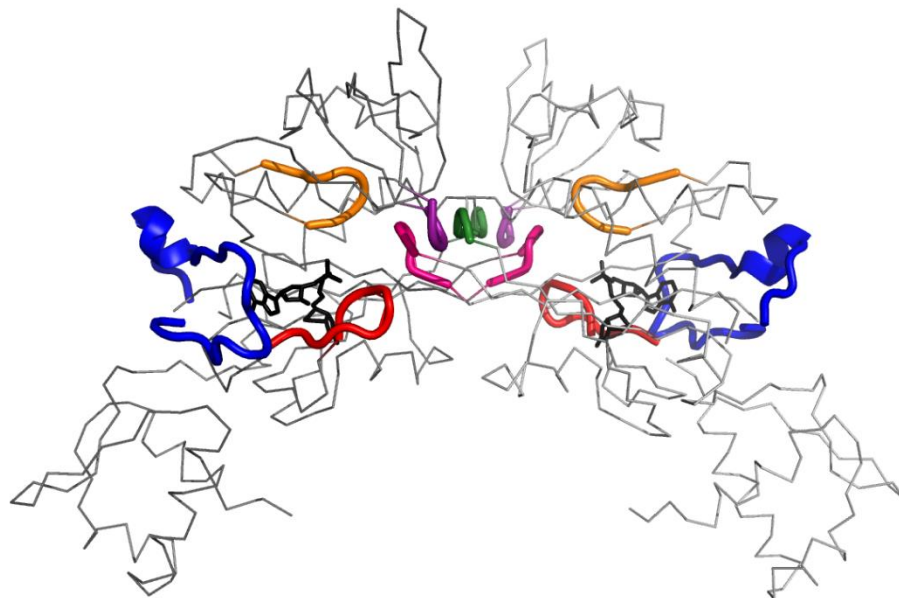
Figure 1.4: Functional loops in the BirA dimer.
Due to their presence on the dimerization surface, alanine substitutions in the 140-143 (green), 194-197, (pink) and 280-283 loops are investigated for their role in allosteric activation.

(Figure 1.4) and the resulting proteins have variable ΔG°_{DIM} values consistent with their roles in BirA dimerization[20](Figure 1.5).

Alanine substitution at residue G142 gives the largest perturbation to the dimerization free energy of 4.4±0.6 kcal/mol. In other words, G142A BirA dimerizes with energetics similar to those measured for apo BirA. This variant is also perturbed in adenylate binding by 3.0±0.4 kcal/mol relative to wild type BirA[19]. Consistent with abolition of coupling between corepressor binding and dimerization, the monomeric structure G142A BirA bound to biotinol-adenylate, a non-hydrolyzable bio-5'-AMP analog, resembles that of wild type apo BirA. Additionally residues 193-199 on the dimerization surface and residues 211-221 in the ABL are disordered in the G142A structure. This provides evidence for the role of coupled disorder-to-order transitions on the two functional surfaces in allosteric activation of the BirA monomer[19].

The data obtained for G142A BirA was the first to functionally demonstrate communication from the dimerization surface to the ligand binding surface. However, it is not known if other residues on the dimerization surface also communicate to the ligand binding surface. This paper further investigates the mechanism of communication from the dimerization to the ligand binding surface in the BirA monomer. By measuring corepressor binding of other alanine-substituted variants in the dimerization surface loops using isothermal titration calorimetry (ITC) titrations, both Gibbs free energy and enthalpy of bio-5'-AMP binding are determined. From these parameters, the entropy change of corepressor binding can be calculated so that the thermodynamic contributions to ligand binding can be discussed. Similar to G142A BirA, significant alterations in bio-5'-AMP binding free energy would

indicate other residues that also functionally communicate to the ligand binding surface.

To further characterize the source of alterations in corepressor binding, the heat capacity change of bio-5'-AMP association was determined by linear regression of the temperature dependence of the binding enthalpy. Binding enthalpies from 10 to 25°C were measured using ITC at total association at partial saturation (TAPS) conditions[21]. The heat capacity change of bio-5'-AMP binding is negative for all variants and significant deviations from that of wild type BirA are observed. Following a correction for the contribution of BirA dimerization, a strong correlation between heat capacity change and the free energy of dimerization is observed for most variants. Residues for which the heat capacity change is more positive are those for which alanine mutagenesis results in the loss of intramolecular interactions on the dimerization surface.
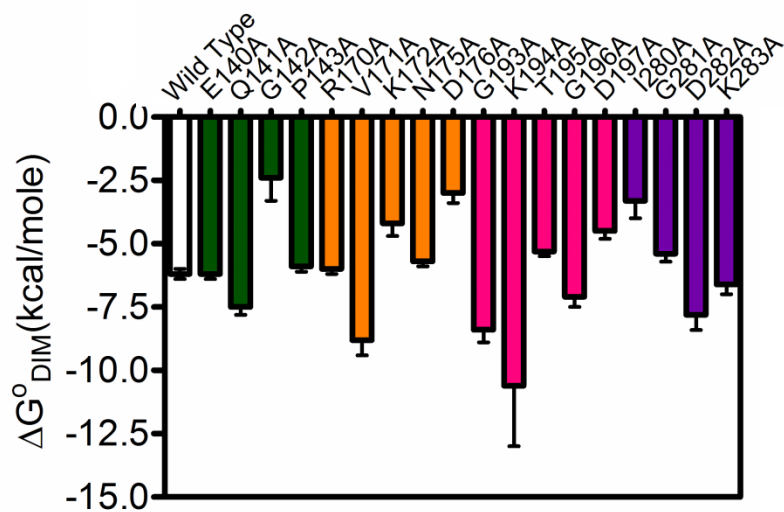
Figure 1.5: BirA·bio-5'-AMP homodimerization free energies of dimerization surface variants.

Homodimerization free energies of bio-5'-AMP bound wild type (white) and single alanine variants in the 140-143 (green), 170-176 (orange), 193-197 (pink), and the 280-283 (purple) dimerization surface loops. Error bars represent the standard deviation from at least two sedimentation equilibrium measurements in 10mM Tris (pH 7.50), 200mM KCl, and 2.5mM MgCl$_2$ at 20°C. Figure adapted from Adikaram, Beckett 2012[20]

Chapter 2 : Materials and Methods

Chemicals and biochemicals

All chemicals and biochemicals used in this study were at least reagent grade. Isopropyl-β-D-1-thiogalactopyranoside (IPTG) was purchased from Teknova and 1M solutions were prepared in MQH20 (Millipore—Milli-Q synthesis, resistance=$18.2M\Omega \cdot cm$) from dry powder immediately prior to use. A 100mM phenylmethylsulfonyl fluoride (PMSF, Sigma) solution was prepared by dissolving the dry powder in 95% ethanol. Luria Bertani (LB) broth for bacterial growth was prepared using 10g/L tryptone (Bacto), 5g/L yeast extract (Bacto), 5g/L NaCl (Mallinckrodt), 0.1% 1M NaOH (Fisher), and was used less than a week after sterilization by autoclaving at 250°F, 22 psi, for 20 minutes. Ampicillin (AMP, Fisher) was prepared as a fresh 100mg/mL solution in MQH_2O immediately before addition to liquid LB media or LB-agar. Polyethylenimine (PEI) was purchased from Sigma and diluted to a 10% working solution in MQH20. This solution was adjusted to a pH of 7.5 with HCl.

Because biotin has no spectral signal, it must be quantitatively prepared so that the concentration can be accurately known. D-biotin was obtained from Sigma-Aldrich and prepared in Standard Buffer (10mM Tris pH 7.5 at 20°C, 2.5mM $MgCl_2$, 200mM KCl). Due to its poor solubility in H20, (0.22mg/mL, or 900μM at 25°C[22]), care was taken to prepare biotin solutions at a concentration well below this value. This ensures the weight of biotin measured accurately represents dissolved biotin and that no undissolved biotin solids are lost upon filtration. Biotin powder was weighed

into a small beaker, in which the stock solutions for 25mL of Standard Buffer (1M Tris Base, 1M $MgCl_2$, 2M KCl) were added. After the addition of 80% of the total volume as MQH_20 to dissolve the lyophilized powder, the pH of the solution was adjusted to 7.50 at 20°C with HCl. Following quantitative transfer to a 25mL volumetric flask, the remaining volume of MQH_2O was added to bring the final volume to 25mL. The biotin solution was subsequently filtered with a 0.22μm mixed-cellulose GSWP filter (Millipore) that was pre-rinsed with MQH_20. Following the filtration, the solution was aliquoted into 1mL fractions and stored at -80°C to minimize oxidation.

The bio-5'-AMP was synthesized and purified in lab as previously described[23,24]. As an anhydride, hydrolysis of bio-5'-AMP to its constituents, biotin and adenosine monophosphate (AMP), can occur. Adenylate integrity was assessed by chromatographic separation on a cellulose F, TLC membrane (EMD) using a mobile phase of 3:2:1 (v:v:v) of amyl alcohol, formic acid, H_20 respectively. Greater than 1nmol of biotin or bio-5'-AMP was visualized with a stain comprised of 1% H_2SO_4, 0.1% p-dimethylcinnemaldehyde solution in 95% ethanol. This solution quickly stains biotin-containing compounds bright pink. Purity was assessed by the presence of only a single bio-5'-AMP band (R_f=0.53).

Expression and purification of BirA variants occurred as previously published[20] except for wild type, E140A, and K283A BirA. These proteins were isolated as described in **Appendix 3: Expression and Purification of BirA Variants**.

Isothermal titration calorimetry (ITC) measurements

All titrations were performed on a Microcal VP-ITC (Malvern) calorimeter with a 1.44mL cell volume. For all experiments, the sample cell contained protein and the 250μL mixing syringe contained the ligand. In each titration, 21-23 injections of ligand were added into the sample cell. Titrations were designed with two factors in mind: first the c-value ($c = K_A P_t n$; where K_A is the association constant, P_t is the total protein concentration, and n is the stoichiometry of ligand binding), for the binding curve was within the recommended range for association constant determination of 5-500 ($500 \geq \frac{P_t \cdot n}{K_D} \geq 5$)[28]. Second, care was taken so that both pre-saturation and post-saturation enthalpy plateaus were represented by several injections. This required the use of a larger number of lower-volume ligand injections. These factors, as well as usage of an experimental design tool[29] are detailed in Appendix 2.

Prior to performing a titration, all protein solutions (200-500uL) were dialyzed twice, the second dialysis overnight, in 250mL of 0.22um-filtered (GSWP) Standard Buffer (10mM Tris pH 7.5 at 20°C, 2.5mM $MgCl_2$, 200mM KCl) at 4°C. To eliminate any precipitate, the protein solution was then filtered with a 0.45um PTFE syringe filter. The concentration of the protein solution was determined using absorbance spectroscopy ($\varepsilon_{M, 280nm}$=47510$M^{-1}cm^{-1}$). During this process the buffer from dialysis was degassed for at least 8 min using the Microcal ThermoVac accessory. To ensure buffer matching, this dialysate was used to dilute both protein and ligand solutions to the appropriate final concentrations (see results). Directly prior to ligand and protein loading, both solutions were degassed for 8-10 minutes in

the Microcal ThermoVac accessory 2-3°C above the working temperature. To further prevent interference from bubble formation/popping during the titration, each experiment was initiated with a 2μL injection to clear the syringe tip. The default stir speed and data filter time of 310 rpm and 2 seconds respectively were used for all titrations. Both the 'Fast Equilibration' and 'Auto Equilibration' options were used with the 'High' gain/feedback setting.

Integration of the raw titration peaks was performed in the Microcal software suite in Origin 7.0; this process consisted of first computer-assisted baseline assignment followed by manual refinement. Multiple analyses of identical titration data indicated little variation in binding parameters. The heat of injection was assumed to be constant for all titrations based on previous biotin and bio-5'-AMP dilution experiments. This heat was calculated from the average value of heats associated with the final 4-5 injections of the titration, which were after protein saturation. Prior to model-fitting, this heat was subtracted from each heat of injection to obtain the heat of ligand binding. Injection heats were normalized to the moles of ligand injected, resulting in the final molar heats of injection. Each isotherm was fit using nonlinear least squares regression to a binding model in Origin 7.0 (see Direct, Displacement, and TAPS titrations below). It was from this regression that the equilibrium constant, molar enthalpy, and stoichiometry of binding was determined.

The sample cell contents were removed following each titration, after which the cell was thoroughly washed with 800mL of working concentration of RBS_{35} detergent (1:50 RBS_{35}:diH_2O) using the Microcal ThermoVac. To remove this detergent, the cell was rinsed with two or three 1L volumes of MQH_2O. When not in

use, the sample cell was filled with MQH$_2$O to prevent both the need for later equilibration in water and the deposition of any residue by evaporation of the cell contents.

Direct ITC binding measurements of biotin binding parameters

The direct binding method was used to determine the binding parameters for the BirA dimerization surface variants to biotin and for BirA variant G142A to bio-5-AMP. The design of direct binding titrations was aided by a spreadsheet-based simulation tool for a single-site binding model[29]. Each biotin titration consisted of twenty-one 7μL injections of 50 μM biotin into a 2.5μM BirA solution and was terminated by a single 100μL injection. This final injection sufficiently saturated BirA with biotin for a following displacement titration (see Displacement ITC). The Bio-5'-AMP direct titrations were performed with twenty 13μL injections of 20 μM bio-5'-AMP into a 2μM BirA solution. For all direct titrations, a 300 second delay between injections was sufficient for complete baseline equilibration. Integration of the resulting injection peaks yields the molar heat of injection, q_i. Following baseline subtraction (see ITC measurements), the isotherms were fit to the single-site binding model:

$$q_i = \frac{nM_t\Delta H°V_0}{2}\left[1 + \frac{X_t}{nM_t} + \frac{1}{nK_AM_t} - \sqrt{\left(1 + \frac{X_t}{nM_t} + \frac{X_t}{nM_t}\right)^2 - \frac{4X_t}{nM_t}}\right]$$

using Origin 7.0 least-squares analysis software to determine the association constant, K_A, binding stoichiometry, n, and molar enthalpy change, $\Delta H°$, of ligand binding.

Displacement ITC binding measurement of bio-5'-AMP binding parameters

Direct measurement of $K_{A, bio-5'-AMP}$ was not possible for several variants due to the corepressor's tight interaction with BirA ($K_{D, bio-5'-AMP} < 10^{-10}$M)[30]. To achieve an adequate c-value for $K_{D,bio-5'-AMP}$ measurement, a nanomolar protein concentration would be required. However, this protein concentration would provide an insufficient heat of binding to distinguish itself from the heat of dilution. Instead, bio-5'-AMP displacement of biotin from saturated BirA was measured. With this method, the apparent association constant, $K_{A, app}$, is within an accessible range. This value is a function of the $K_{A, Biotin}$ (see direct binding) and $K_{A, bio-5'-AMP}$, as well as the bulk biotin concentration, [biotin].

$$K_{app} = \frac{K_{A,bio5'AMP}}{1 + K_{A,biotin}[biotin]}$$

Similarly, the enthalpy of bio-5'-AMP binding can be deconvoluted from the apparent measured binding enthalpy using the following expression in which $\Delta H°_{biotin}$ has been previously measured by a direct titration.

$$\Delta H°_{app} = \Delta H°_{bio5'AMP} - \Delta H°_{biotin} \frac{K_{A,biotin}[biotin]}{1 + K_{A,biotin}[biotin]}$$

However, binding enthalpies determined by this method were not used in analysis of the titration data (see appendix 1). Instead, those values obtained from direct TAPS titrations were used.

Displacement titrations were designed so that upon injection, bio-5'-AMP displaces biotin at its shared binding site on BirA. To ensure complete biotin saturation prior to titration, a 6μM final biotin concentration was used ([biotin]>$K_{D,}$

Biotinx100), which was achieved at the end of each direct titration. To perform each displacement titration, twenty-one 12µL injections of 22µM bio-5'-AMP and 6µM biotin were titrated into the sample cell, containing 2.2µM BirA and 6µM biotin. Due to the slower kinetics of the displacement reaction, a longer, 360 second, equilibration period was required between injections.

Total association at partial saturation (TAPS) calorimetry

Calorimetric titrations in TAPS conditions[21] were utilized to measure $\Delta H_{bio-5'-AMP}$ at temperatures ranging from 10°C-25°C for the purpose of calculating the molar heat capacity of corepressor binding. This method allows for more accurate determination of the binding enthalpy by decoupling it from the equilibrium association constant. TAPS conditions are achieved at high c-values (when $\frac{P_t n}{K_D}>500$), at which there is complete binding upon ligand injection, for multiple injections. Because of the large dependence of pKa_{tris} on temperature, the pH of standard buffer used was adjusted using HCl to pH=7.5 at each working temperature. The faster kinetics of direct binding permitted a 300 second delay between injections. For all TAPS titrations, five 7µL injections of 20µM bio-5'-AMP are followed by a single, saturating, 180µL injection and terminated by six 10µL injections. The integrated heat from the first five injections represents the sum of the heat of binding and heat of dilution, $\Delta H°_{tot}$.

$$\Delta H°_{tot} = \Delta H°_{bio-5'-AMP} + \Delta H°_{dil}$$

The final six injections represent the molar heat of dilution, ΔH_{dil}. The difference of these terms yields the enthalpy of bio-5'-AMP binding:

$$\Delta H^{\circ}{}_{bio-5'-AMP} = \Delta H^{\circ}{}_{tot} - \Delta H^{\circ}{}_{dil}$$

By subtraction of the average experimental heat of dilution, five measurements of the molar enthalpy, corresponding to the five pre-saturation injections, were obtained at each temperature.

Molar heat capacity changes of bio-5'-AMP binding

Heat capacity changes of bio-5'-AMP binding by the BirA variants were calculated using the $\Delta H_{bio\text{-}5'\text{-}AMP}$ values from the ITC-TAPS titrations above. The heat capacity change, $\Delta C^{\circ}{}_P$, is the slope of the linear enthalpy versus temperature relationship, $\Delta H^{\circ} = q_P = \Delta C_P{}^{\circ} \cdot \Delta T$, as determined by linear regression. Each calculation of $\Delta C^{\circ}{}_p$ was comprised of five enthalpies of bio-5'-AMP binding at each of four temperatures, 10°C, 15°C, 20°C, 25°C.

Chapter 3 : Results

Allosteric activation of BirA for dimerization occurs via communication of disorder-to-order transitions at the corepressor binding and dimerization surfaces. This was communication was further investigated by measuring the ligand binding properties of dimerization surface variants using isothermal titration calorimetry (ITC).

Selection of alanine-substituted dimerization surface variants

BirA variants with alanine substitutions in four dimerization surface loops reveal a range of effects (**Figure 1.5**) on the equilibrium dimerization constant[20]. A subset of these variants was selected for ligand binding measurements based on the following criteria:

Variants in the 170-176 dimerization loop were not studied due to their proximity to the active site and known role in catalysis[20]. In the remaining three loops, only variants with dimerization affinities similar to or lower than that measured for wild type BirA were studied. This approach was adopted to target variants that, like G142A BirA, are more likely to be defective in communication to the ligand binding surface. Moreover, weak dimerization also minimizes contributions from the 41 ± 3 kcal/mol homodimerization enthalpy to the ITC measurements[31]. Using these criteria, variants E140A, G142A, P143A, T195A, G196A, D197A, I280A, G281A, and K283A were selected. The dimerization energetics of these variants are summarized in Table 3.1.

BirA variant	K_{dim} (M)[a]	ΔG^{o}_{dim} (kcal/mol)[a]
Wild Type	$7(\pm3)x10^{-6}$	-6.8 ± 0.3
E140A	$22(\pm5)x10^{-6}$	-6.2 ± 0.2
G142A	$17(\pm52)x10^{-3}$	-2.4 ± 0.9
P143A	$4(\pm1)x10^{-5}$	-5.9 ± 0.2
T195A	$10(\pm4)x10^{-5}$	-5.3 ± 0.2
G196A	$5(\pm4)x10^{-6}$	-7.1 ± 0.4
D197A	$5(\pm3)x10^{-4}$	-4.5 ± 0.3
I280A	$4(\pm3)x10^{-3}$	-3.3 ± 0.7
G281A	$9(\pm4)x10^{-5}$	-5.4 ± 0.3
K283A	$12(\pm7)x10^{-6}$	-6.6 ± 0.4

Table 3.1: Homodimerization energetics of chosen BirA variants:
Errors represent the standard deviation from at least two sedimentation equilibrium measurements in 10mM Tris (pH 7.50), 200mM KCl, and 2.5mM $MgCl_2$ at 20°C.[20]

Dimerization loop variants bind biotin with affinities similar to wild type BirA

As a control for the presence of non-allosteric effects on ligand binding, such as loss of binding site integrity, biotin binding to all variants was measured. Since this ligand does not elicit an allosteric response[16], perturbations to biotin binding are unlikely to reflect effects on inter-surface communication. Thermodynamic parameters of biotin binding were obtained by direct ITC binding titrations. See materials and methods for experimental details.

ITC titration data for biotin binding to I280A BirA are shown in Figure 3.1. Analysis of the data indicated excellent agreement to a single site binding model, yielding the dissociation constant, molar enthalpy, and stoichiometry of biotin binding from which the Gibbs free energy, $\Delta G°_{biotin}$, and entropy, $-T\Delta S°_{biotin}$ were calculated. The values of these parameters for the I280A variant (**Table 3.2**) are identical, within one standard deviation, to those obtained for wild type BirA.

Biotin binding titrations performed on all other variants yielded data that are also well described by a single site model. Moreover, the thermodynamic parameters obtained from analysis of the titration data are, with few exceptions, equivalent to those obtained for wild type BirA (**Table 3.2**). For all variants, the equilibrium dissociation and Gibbs free energy of binding are identical and the same as those obtained for wt BirA. However, the thermodynamic contributions to the free energy of binding for G142A BirA differ from those obtained for wild type BirA. The molar binding enthalpy for this variant is -1.8 ±0.4kcal/mol more favorable than wild type
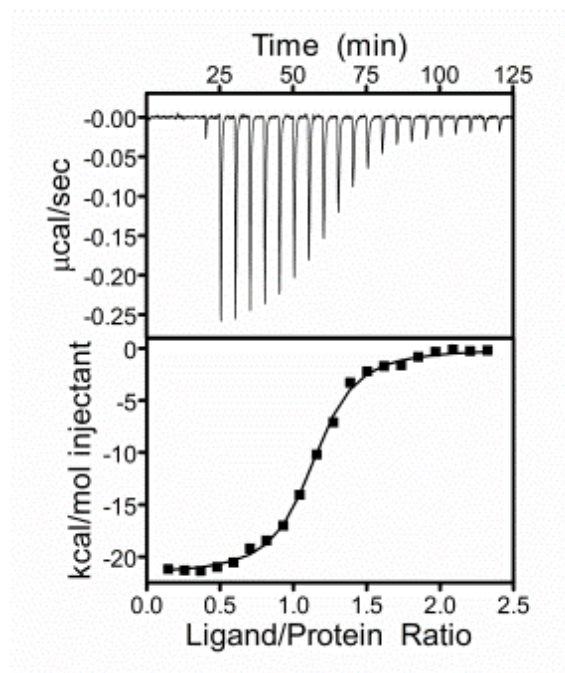
Figure 3.1: Direct biotin titration of I280A BirA.

This figure illustrates data for the direct binding ITC method. Each titration was performed by injecting twenty 7uL injections of 50 µM biotin into 1.44mL of BirA. Both protein and ligand solutions were prepared in 10mM Tris (pH=7.50 at 20°C), 200mM KCl, and 2.5mM MgCl$_2$. The top panel is the ITC data trace following manual baseline correction. After integration and normalization to the moles of injectant, the binding isotherm, bottom panel, is obtained. The binding isotherm for I280A BirA is fit to a single site model for the biotin binding parameters.

Table 3.2: Thermodynamic parameters of biotin binding for BirA variants

Protein	K_D (M)	$\Delta G°$ (kcal/mol)	$\Delta H°$ (kcal/mol)	$-T\Delta S°$ (kcal/mol)	N
wild type	$4.7(\pm0.8)\times10^{-8}$	-9.8±0.1	-20.1±0.4	10.3±0.5	0.93±0.01
E140A	$4.0(\pm0.4)\times10^{-8}$	-9.92±0.05	-20.1±0.2	10.2±0.2	0.931±0.006
G142A	$4.0(\pm0.4)\times10^{-8}$	-9.92±0.06	-21.9±0.2	12.0±0.3	1.085±0.009
P143A	$4.5(\pm0.3)\times10^{-8}$	-9.85±0.04	-19.7±0.1	9.9±0.1	0.955±0.004
T195A	$4.5(\pm0.5)\times10^{-8}$	-9.85±0.06	-19.9±0.2	10.1±0.2	0.894±0.007
G196A	$5.1(\pm0.5)\times10^{-8}$	-9.78±0.06	-20.3±0.2	10.5±0.2	0.984±0.007
D197A	$4.2(\pm0.4)\times10^{-8}$	-9.89±0.05	-20.1±0.2	10.2±0.5	1.260±0.008
I280A	$4.6(\pm0.5)\times10^{-8}$	-9.84±0.06	-20.6±0.2	10.8±0.2	1.027±0.007
G281A	$4.1(\pm0.4)\times10^{-8}$	-9.91±0.05	-20.4±0.2	10.5±0.2	0.878±0.006
K283A	$3.9(\pm0.2)\times10^{-8}$	-9.93±0.03	-20.8±0.3	10.8±0.3	0.904±0.009

Measured at 20°C by direct ITC titration in 10mM Tris (pH=7.50 at 20°C), 200mM KCl, 2.5mM MgCl$_2$. Each parameter represents the average from at least two independent measurements. The uncertainty provided is the propagated 68% confidence interval from the nonlinear-least-squares regression to a single site model.

A.
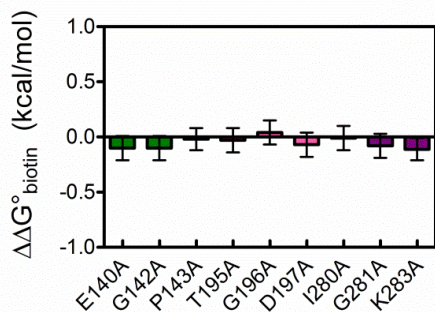
B.
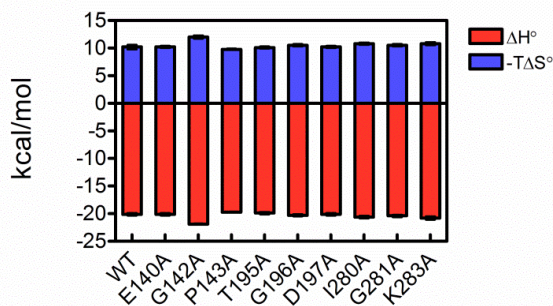
Figure 3.2: Comparison of thermodynamic parameters of biotin binding for BirA variants. A) Change in the Gibbs free energy of biotin binding, $\Delta\Delta G°_{biotin, variant} - \Delta\Delta G°_{biotin, wt}$, shown for the nine variants. Error bars shown represent propagated 68% confidence intervals from wild type and the appropriate variant. B) The enthalpic (red) and entropic (blue) components of the biotin binding free energy for each BirA variant at 20°C. Errors bars shown are the propagated 68% confidence intervals resulting from nonlinear least squares analysis.

BirA. Additionally, the entropic component of binding, $-T\Delta S^\circ_{biotin}$, is 1.7 ± 0.6 kcal/mol less favorable. Nonetheless, the free energy of biotin binding remains equivalent to that of wild type at -9.92 ± 0.06 kcal/mol.

With one exception, the resolved stoichiometries of biotin binding range from 0.878 and 1.085 are consistent with a 1:1 binding stoichiometry. The exception, BirA D197A, yields a reproducibly higher value of 1.260 ± 0.008. Since this value is consistent with results of stoichiometric titrations monitored by fluorescence, (unpublished data) this behavior appears to be an intrinsic property of the variant.

Alanine substitution at residue G142 greatly perturbs bio-5'-AMP binding.

The perturbed ABL folding of the G142A BirA variant indicates functional communication from the BirA dimerization surface to the ligand binding surface[32]. The alanine-substituted variants that are also defective in dimerization were analyzed to determine if this communication, measured by loss of bio-5'-AMP binding affinity, extends to other residues on the dimerization surface.

Because of the high c-values that would be required, the affinity $(K_{D,bio\text{-}5'\text{-}AMP} = 5(\pm2)\text{x}10^{-11}\text{M})$ of bio-5'-AMP to wild type BirA precludes the use of direct binding ITC titrations. Therefore, it was necessary to perform corepressor binding measurements using the displacement titration method[33].

For this experiment, biotin-saturated BirA is titrated with bio-5'-AMP which displaces biotin in the course of binding. Nonlinear least squares analysis of this isotherm using a single site model yields the apparent binding parameters used to calculate (see Materials and Methods) the bio-5'-AMP binding parameters.

Data obtained for the I280A BirA displacement titration are shown in **Figure 3.3**. In contrast to biotin binding, this titration is endothermic in its initial injections. This is because the positive enthalpy of biotin release is larger in magnitude than the negative enthalpy of bio-5'-AMP binding. Consequently, the apparent molar binding enthalpy for these measurements was about +6kcal/mol, compared to -20 kcal/mol for the direct biotin binding titrations. This results in a lower signal-to-noise for the parameters obtained using the competitive binding method. Nonetheless, the data are well described by the single site model. Moreover, the thermodynamic parameters of bio-5'-AMP binding (**Table 3.3**) derived from the analysis indicate that I280A BirA is characterized by corepressor binding parameters identical to those determined for wild type BirA.

Displacement titrations were used to measure bio-5'-AMP binding to all variants with the exception of G142A BirA. These measurements yielded free energies of bio-5'-AMP binding (**Figure 3.4**A) identical, within one standard deviation, to that of wild type BirA. The direct titration of G142A BirA with the corepressor indicated much weaker binding with an equilibrium dissociation constant of $8(\pm1) \times 10^{-9}$ M, approximately 160-fold greater than that measured for wt BirA.

The enthalpies of ligand binding obtained by displacement titration were deemed innacurate (see appendix 1) and therefore are excluded from these results. The enthalpies derived from TAPS titrations give insight into the effects observed in the variants. In contrast to the Gibbs free energies of binding, the BirA variants display variable enthalpic and entropic components to bio-5'-AMP binding, illustrated in **Figure 3.4**B. The loss of corepressor binding affinity for G142A BirA compared to
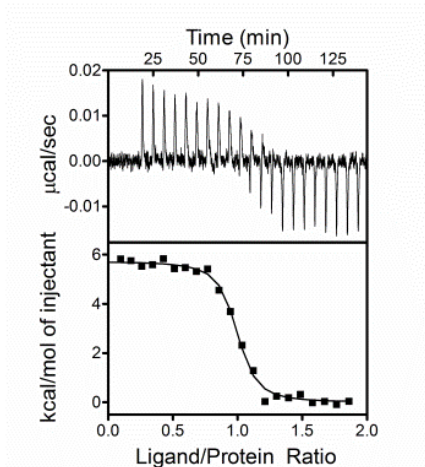
Figure 3.3: Biotin Displacement bio-5'-AMP titration of I280A BirA.
This figure illustrates data for the competitive binding ITC method. Each titration was performed by injecting 20-22, 12uL injections of 22 µM bio-5'-AMP into 1.44mL of BirA. Both protein and ligand solutions were prepared in 10mM Tris (pH=7.50 at 20°C), 200mM KCl, 2.5mM MgCl$_2$, and 6µM biotin. The top panel is the ITC data trace following manual baseline correction. Following integration and normalization to the moles of injectant, the binding isotherm, bottom panel, is obtained. The binding isotherm for I280A BirA is fit to a single site model for the apparent binding parameters from which the bio-5'-AMP binding parameters are calculated

Table 3.3: Thermodynamic parameters of bio-5'-AMP binding.

Protein	K_D (M) [a]	$\Delta G°$ [b] (kcal/mol)	$\Delta H°$ [c] (kcal/mol)	$-T\Delta S°$ [d] (kcal/mol)	n [a]
wild type	3($\pm$3)x10^{-11}	-14.1$\pm$0.5	-12.6$\pm$0.3	-1.4$\pm$0.5	1.06$\pm$0.02
E140A	7($\pm$3)x10^{-11}	-13.6$\pm$0.2	-12.43$\pm$0.06	-1.2$\pm$0.2	0.90$\pm$0.01
G142A	8 ($\pm$1)x10^{-9}	-10.85$\pm$0.09	-13.3$\pm$0.1	2.9$\pm$0.2	1.01$\pm$0.01
P143A	8($\pm$2)x10^{-11}	-13.5$\pm$0.2	-12.2$\pm$0.01	-1.4$\pm$0.2	0.96$\pm$0.01
T195A	10($\pm$4)x10^{-11}	-13.4$\pm$0.2	-12.58$\pm$0.07	-0.9$\pm$0.2	0.88$\pm$0.01
G196A	2($\pm$3)x10^{-11}	-14.2$\pm$0.8	-11.90$\pm$0.1	-2.4$\pm$0.8	1.09$\pm$0.03
D197A	9($\pm$3)x10^{-11}	-13.5$\pm$0.2	-12.43$\pm$0.2	-1.1$\pm$0.3	1.21$\pm$0.02
I280A	9($\pm$2)x10^{-11}	-13.5$\pm$0.1	-12.5$\pm$0.1	-0.9$\pm$0.2	1.06$\pm$0.01
G281A	8($\pm$3)x10^{-11}	-13.6$\pm$0.2	-12.7$\pm$0.2	-0.9$\pm$0.3	0.89$\pm$0.01
K283A	9($\pm$2)x10^{-11}	-13.5$\pm$0.3	-13.3$\pm$0.2	-0.2$\pm$0.2	0.89$\pm$0.01

Above binding parameters were measured at 20°C by displacement ITC titration in 10mM Tris (pH=7.50 at 20°C), 200mM KCl, 2.5mM MgCl$_2$. Each parameter represents the average from at least two independent measurements. Uncertainty provided is the propagated 68% confidence interval from the nonlinear-least-squares regression to a single site model.
[a] Obtained from nonlinear least squares analysis of displacement titration data to a single site binding model in Origin 7.0.
[b] Enthalpy obtained from direct TAPS titration at 20°C.
[c] Entropy, -TΔS°, calculated using the expression $\Delta G°=\Delta H°-T\Delta S°$
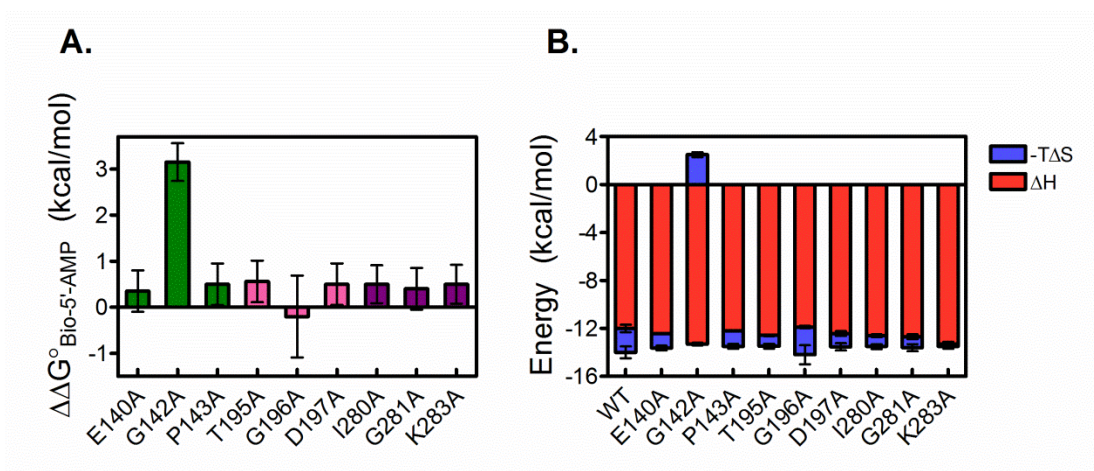
Figure 3.4: Energetic contribution to bio-5'-AMP binding for BirA variants.
A) Change in the Gibbs free energy of bio-5'-AMP binding, $\Delta\Delta G°_{bio-5'-AMP, variant}$-$\Delta\Delta G°_{bio-5'-AMP, wt}$, for the nine variants studied. Error bars are the propagated uncertainties from both wild type and appropriate variant. B) The enthalpic (red) and entropic (blue) components of the free energy of bio-5'-AMP binding for each BirA species studied. Errors bars shown are the propagated 68% confidence intervals.

wild type reflects both a modestly more favorable $\Delta H°_{G142A,}$ by -0.g237±0.3 kcal/mol

, and less favorable $-T\Delta S°_{G142A}$ of 4.3±0.5 kcal/mol. In agreement with the biotin

binding measurements, the stoichiometries of bio-5'-AMP binding, shown in Table

3.3, are consistently between 0.89 and 1.09, except for variant D197A

$\Delta C°_{p,bio-5'-AMP}$ is more negative for BirA dimerization surface variants

To further probe the structural basis of the BirA allosteric mechanism, the

heat capacity changes associated with bio-5'-AMP binding to the variants were

determined from measurements of the temperature dependence of the enthalpy of

ligand binding. For each protein, the enthalpy of bio-5'-AMP binding was measured

between 10°C and 25°C using the ITC total association at partial saturation (TAPS)

method[21].

TAPS titration data for BirA variant G196A are shown in **Figure 3.5**.

Analogous to the direct biotin titration in **Figure 3.1**, the initial five injections, when

integrated, represent the combined heats of ligand binding and ligand dilution. A

large injection of bio-5'-AMP then saturates the protein so that the remaining six

injections only measure the heat of ligand dilution. The difference in the heats for

these injections, when normalized to the ligand concentration, yields the molar

enthalpy of binding. Therefore, from a single titration, five measurements of the bio-

5'-AMP binding enthalpy were obtained.

Linear regression of this data for G196A BirA yields a heat capacity change

associated with bio-5'-AMP binding of -240±6 cal/mol·K. The r^2 value of the linear

regression, 0.95, indicates the heat capacity change was constant over the temperature

range used.

Linear regression of the molar bio-5'-AMP binding enthalpy versus temperature data for the remaining BirA variants (**Table 3.4**) indicated a constant heat capacity over the temperature range employed as judged by r^2 values ranging from 0.91 to 0.98. The $\Delta C^\circ_{p,bio\text{-}5'\text{-}AMP}$ is more negative for all variants than the value obtained for wild type. The $\Delta C^\circ_{p, bio\text{-}5'\text{-}AMP}$ values are, within one standard deviation, identical within the 280-283 loop. Additionally, no significant differences in $\Delta C^\circ_{p, bio\text{-}5'\text{-}AMP}$ are observed among variants E140, P143A, T195A and D196A. The tightest dimerizing variant, G196A BirA, has the most positive heat capacity but, G142A BirA, which has the following most positive $\Delta C^\circ_{p,bio\text{-}5'\text{-}AMP}$, is most defective in dimerization.
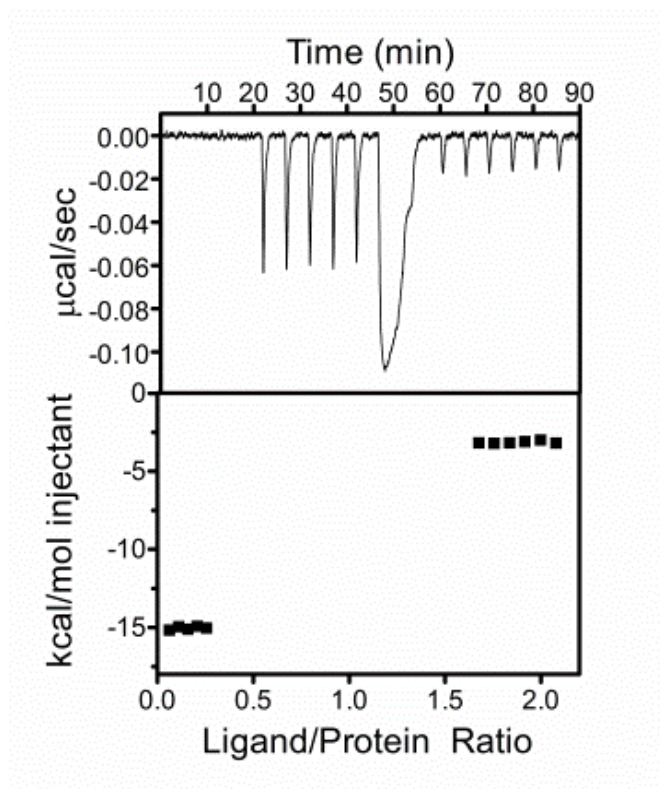
Figure 3.5: Bio-5'-AMP TAPS titration of G196A BirA
Each titration was performed by injecting first five, 7μL injections of 20 μM bio-5'-AMP into 1.44mL of BirA. To saturate the protein solution, 180μL of 20μM bio-5'-AMP were injected. After saturation, six 10μL injections of 20 μM bio-5'-AMP were performed. Both protein and ligand solutions were prepared in 10mM Tris (pH=7.50 at 20°C), 200mM KCl, 2.5mM $MgCl_2$. The top panel is the ITC data trace following manual baseline correction. After integration and normalization to the moles of injectant, the binding isotherm, bottom panel, is obtained. The difference between the molar heat before and after protein saturation provides the enthalpy of ligand binding.
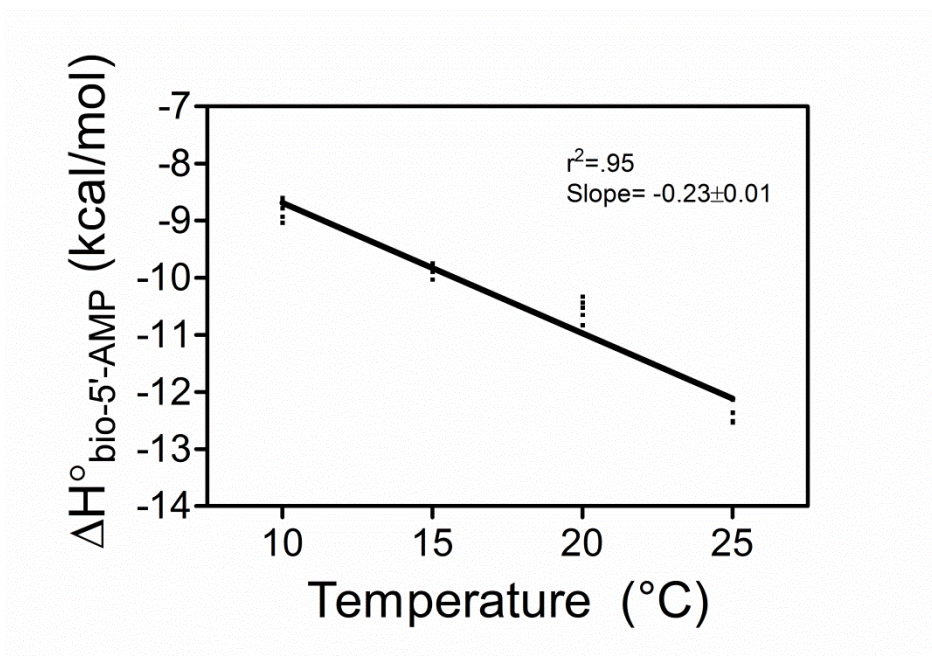
Figure 3.6: Heat capacity change of bio-5'-AMP binding for G196A BirA.
The heat capacity change was obtained from the slope of linear least squares regression of the enthalpy-temperature relationship, $\Delta C_p° = \frac{\Delta H°}{\Delta T°}$. Either four or five measurements of ΔH°$_{bio-5'-AMP}$ were obtained at each temperature by a single ITC-TAPS titration at 10, 15, 20, and 25°C.

Table 3.4: Heat capacity change of bio-5'-AMP binding for BirA dimerization surface variants.

Protein	ΔC_P [a] (kcal/mol·K)	$\Delta\Delta C_P$ (kcal/mol·K)
wild type	-0.30±0.01	—
E140A	-0.37±0.03	-0.07±0.01
G142A	-0.300±0.008	-0.00±0.03
P143A	-0.363±0.008	-0.06±0.01
T195A	-0.37±0.01	-0.07±0.01
G196A	-0.240±0.006	0.06±0.01
D197A	-0.364±0.009	-0.06±0.01
I280A	-0.31±0.01	-0.01±0.01
G281A	-0.31±0.01	-0.01±0.01
K283A	-0.29±0.02	0.01±0.02

Calculated from linear regression of the temperature dependence of $\Delta H°_{bio-5'-AMP}$ (Figure 3.6). Uncertainty given in $\Delta C°_p$ is the 68% confidence interval from linear regression. Change in $\Delta C°_p$ from wild type, $\Delta\Delta C°_p$, is calculated by $\Delta C°_{p,variant} - \Delta C°_{p,wt}$. Uncertainty in $\Delta\Delta C°_p$ is the propagated error in heat capacity change for wild type and the BirA variant.
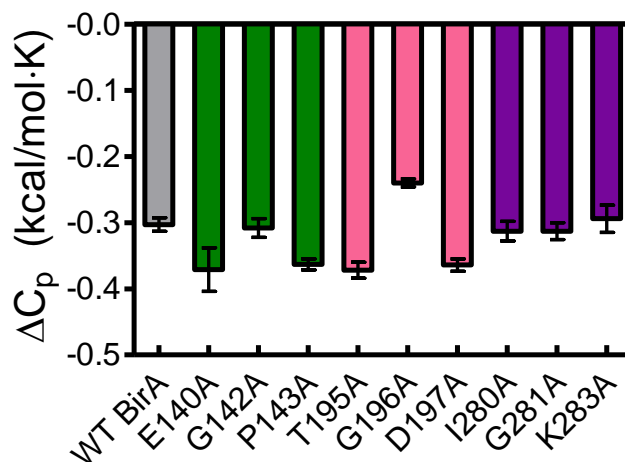
Figure 3.7: Comparison of heat capacity change measurements.
The $\Delta C°_p$ of wild type (grey), upon alanine substitution in the 140-143 loop (green), the 193-197 loop (pink) and the 280-283 loop (purple). Error bars are the standard deviation of the slope from linear regression

Chapter 4 : Discussion

The loss of Gibbs free energy of both dimerization and bio-5'-AMP binding measurements in G142A BirA indicate that coupling between ligand binding and dimerization has been abolished. Of the alanine substitutions introduced on the dimerization surface, only G142A results in defective bio-5'-AMP binding indicating disruption of elements critical for site-to-site communication in the wild type protein. Consistent with the role of disorder-to-order transitions in allosteric activation of the BirA monomer, the G142A crystal structure indicates an unfolded ABL and 193-197 loop. Additionally, N-terminal extension of the 147-164 helix by four residues that is observed in wild type BirA upon corepressor binding is not observed in the G142A structure.

Large heat capacity changes upon bio-5'-AMP binding for the variants indicate that although communication to the ligand binding surface is not observed for the remaining residues, perturbations to the dimerization surface are present and correlate well with the resulting effects on BirA dimerization free energy. Moreover, these results are consistent with formation of intramolecular interactions upon loop folding being critical for the modulation of dimerization free energy.

BirA integrity is maintained upon alanine substitution

Alanine substitutions in all dimerization surface variants elicit no observable penalty to the free energy of biotin binding. Therefore, it is reasonable to assume that there is no large conformational change or loss of protein stability resulting from mutagenesis that would functionally disturb bio-5'-AMP binding. This assumption is

further supported by the BirA G142A crystal structure which demonstrates retention of secondary structural elements present in apo BirA and the holo BirA monomer. Moreover, alanine substitutions in the ABL induced deficient bio-5'-AMP binding without disturbing the free energy of biotin binding[18]. Therefore, because alanine substitutions in these flexible loops do not indicate disruption of the protein structure, any alteration to the Gibbs free energy of bio-5'-AMP binding upon alanine substitution can be considered due to perturbation of long distance allosteric communication.

Residue G142 displays evidence for communication to the ligand binding site

The free energy of bio-5'-AMP binding is only perturbed by alanine substitution at residue G142. As discussed above, this result demonstrates perturbation of a long distance communication from the dimerization loop residues to the ligand binding surface. Therefore, the structural differences observed in G142A BirA represent perturbations to the features of the allosteric activation of BirA (**Figure 4.1**). The 193-197 loop remains folded in the G142A structure and alanine substitutions in this region do not perturb ligand binding. Therefore the folding of residues 193-197 is not a direct consequence of ABL folding. Instead, it must be influenced by other local effects, such as intramolecular interactions that form as a consequence of the 143-146 alpha helical extension. However, it is not clear how this alpha helical extension is communicated from the ligand binding surface.

Correction of enthalpy of bio-5'-AMP binding for holoBirA dimerization

Titration data indicate that all variants except for G196A have different energetic contributions to bio-5'-AMP binding than wild type. Variant G196A is unique in that it is the only protein with a more favorable dimerization free energy than wild type BirA. Because of the linkage between corepressor binding and dimerization, dimer assembly is a complicating factor in the analysis of ITC-derived binding enthalpies. Moreover, because of the large positive enthalpy of dimerization, 41±3 kcal/mol[31], low quantities of dimer formation contributes significantly to the measured heats. For this reason, despite designing the experiments to minimize this effect, a correction for the heat of dimerization was performed on the measured enthalpies of bio-5-AMP binding.

The fraction of BirA dimer, χ_{DIM}, was calculated for each variant at the total protein concentration, P_{tot}, at the end of each titration. This calculation was performed using the following expression and the equilibrium dimerization constants, $K_{A,DIM}$, previously measured at 20°C[20]:

$$\chi_{DIM} = 1 - \chi_{monomer} = 1 - \frac{-1 + \sqrt{1 + 8K_{A,DIM}P_{tot}}}{4K_{A,DIM}P_{tot}}$$
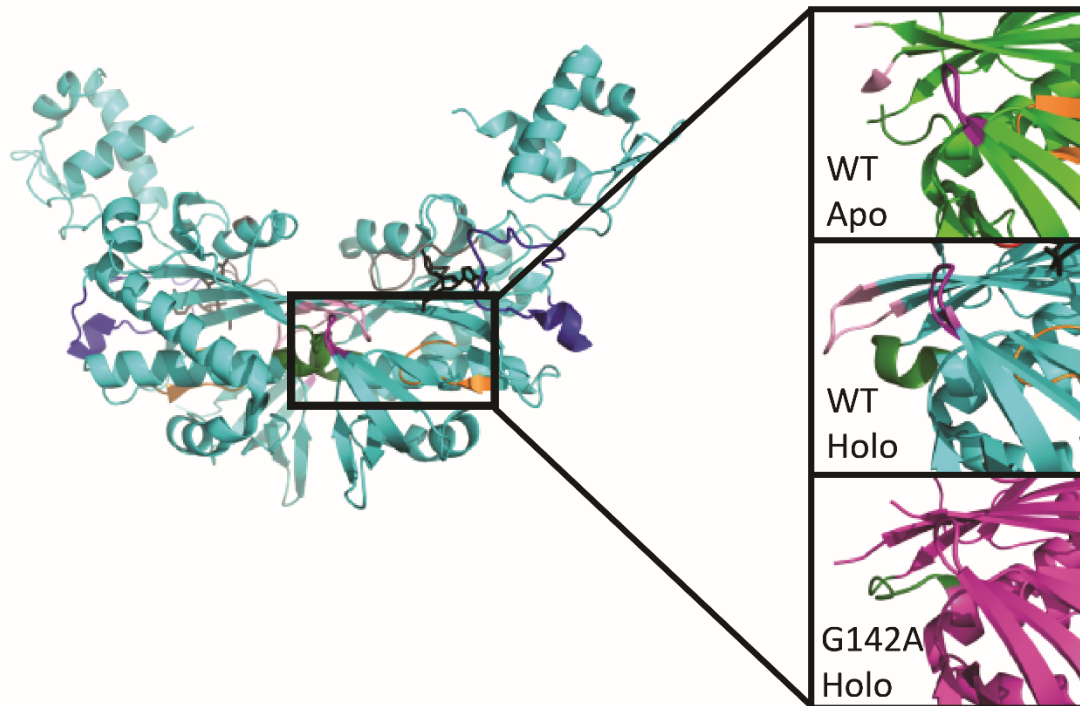
Figure 4.1: Structural comparison of G142A BirA to wild type BirA.
Structural features of the dimerization surface are compared between wt apo (pdb entry 1BIA), wt holo (2EWN), and G142A (4WF2) BirA. Folding of the 193-197 loop (pink) is dependent on the alpha helical extension observed in residues 143-146 (dark green). It should be noted, however, that this is in context of the holoBirA dimer (left).

At the protein concentrations used, at least 10% dimer was present in wild type BirA and variants G196A, K283A, and E140A BirA (**Figure 4.1**)

Therefore, the experimental contribution from BirA dimerization, q_{dim}, to the measured heat of injection, q_{inj}, is:

$$q_{inj} = q_{dim} + q_{bio-5'-AMP}$$

where $q_{bio-5'-AMP}$ is the desired parameter, heat due to ligand binding. This value was calculated using the equation:

$$q_{dim} = \Delta H°_{dim} \cdot [BirA_2]$$

$$= \Delta H°_{dim} \left([holoBirA] - \frac{-1 + \sqrt{1 + 8K_{A,DIM}[holoBirA]}}{4K_{A,DIM}} \right)$$

using the enthlapy of BirA dimerization, $\Delta H°_{dim}$, obtained for wild type BirA. The incremental change in ligand-bound protein concentration, [holoBirA], was equal to the incremental ligand concentration calculated by the Microcal VP-ITC software due to stoichiometric binding conditions. The dimerization constants for each variant, $K_{A,dim}$, are known at 20°C[20], and were determined at the remaining temperatures using the wild-type BirA temperature dependence[31]. To determine the enthalpy of binding, the measured heat due to bio-5'-AMP binding is normalized to the moles of injectant using the following equation:

$$\Delta H°_{bio-5'-AMP} = \frac{q_{bio-5'-AMP} \cdot C_{inj}}{V_{inj}}$$

Where C_{inj} is the concentration of the ligand solution and V_{inj} is the volume of each injection.

By performing this correction, it is assumed that the enthalpy of dimerization of the BirA variants was constant and identical to that measured for wild type BirA.

The basis for this assumption is that measurements of the effect of replacing H_2O

with D_2O are consistent with solvent release serving as the molecular origin of this

large positive enthalpy[34]. Because similar isotope effects are observed on the

dimerization free energies of T195A and V219A BirA, it seems reasonable to assume

ΔH_{DIM} does not differ dramatically from that of wild type despite their free energy

penalties to dimerization.

Correcting for dimerization reveals binding enthalpies for wild type and

G196A BirA now more consistent with the other variants (**Figure 4.2**). The entropy

of binding is revealed to be unfavorable for wild type, G196A, and K283A BirA. This

enthalpy-entropy compensation phenomenon, in which large variations in

thermodynamic parameters lead to little or no change in $\Delta G°_{binding}$ has been seen in

other systems in which small perturbations are made to interacting species[35,36].

In G142A BirA, the loss of free energy stems from a less favorable enthalpy

by 2±1 kcal/mol compared to wild type and a more negative, but within error, $-T\Delta S°$

by 1±1 kcal/mol. A less favorable binding enthalpy is also observed in T195A,

D197A, I280A, and G281A BirA, each of which dimerizes at least 1 kcal/mol less

favorably than wild type. This loss of binding enthalpy may represent the inability to

Table 4.1:Fraction of BirA dimer present in ITC titrations

BirA variant	Fraction Dimer
Wild Type	0.272
E140A	0.125
G142A	0.000
P143A	0.077
T195A	0.034
G196A	0.327
D197A	0.007
I280A	0.001
G281A	0.037
K283A	0.195

Fraction dimers above were calculated using the expression:

$$\chi_{DIM} = 1 - \chi_{monomer} = 1 - \frac{-1 + \sqrt{1 + 8K_{A,DIM}P_{tot}}}{4K_{A,DIM}P_{tot}}$$

at 1.8uM BirA, the average concentration at the end of the TAPS measurements performed. The Dimerization parameters used were obtained from Adikaram 2012[20]

optimize electrostatic interactions on the dimerization surface upon allosteric activation. Although the observed changes in bio-5'-AMP binding enthalpy could also reflect structural changes on the ligand binding surface, all hydrogen bonding interactions to the ligand remain present in G142ABirA and the ligand binding affinity remains unchanged despite the enthalpic penalty in the remaining variants (**Figure 4.2**,**Table 4.2**). For this reason it appears the loss of dimerization free energy stems from disrupting intramolecular interactions on the dimerization surface of the monomer.

$\Delta C^{\circ}_{p,bio-5'-AMP}$ values directly correlate to BirA dimerization

All BirA variants show a more negative heat capacity change of bio-5'-AMP binding than wild type and G196A BirA. Additionally, no correlation is observed between heat capacity change and dimerization free energy of each variant (**Figure 4.5**A) .However, because the heat capacity changes were derived from the enthalpies of bio-5'-AMP binding, the heat of BirA dimerization is also a consideration. Therefore, the correction was performed as above for the binding enthalpies at each temperature obtained by ITC TAPS titrations. Due to the temperature dependence of BirA dimerization[31], the $K_{D,DIM}$ at each temperature was calculated from the variant's dimerization free energy at 20°C. This was performed by using the Van't Hoff equation, assuming the BirA temperature dependence of dimerization was conserved upon alanine mutagenesis. The corrected heat capacity changes (

Figure 4.3,**Table 4.3**) remain negative but are higher in magnitude compared to the non-corrected values. It is revealed that wild type, K283A, and G196A BirA have the most negative heat

38

Table 4.2: Corrected thermodynamic parameters of bio-5'-AMP binding to dimerization surface variants

Protein	$K_D(M)$ [a]	$\Delta G°$ [a] (kcal/mol)	$\Delta H°$ [b] (kcal/mol)	$-T\Delta S°$ [c] (kcal/mol)	n [a]
wild type	$3(\pm3)\times10^{-11}$	-14.1±0.5	-15±1	1±1	1.06±0.02
E140A	$7(\pm3)\times10^{-11}$	-13.6±0.2	-13.7±0.5	0.0±0.5	0.90±0.01
G142A	$8(\pm1)\times10^{-9}$	-10.85±0.09	-13.2±0.1	2.3±0.2	1.010±0.01
P143A	$8(\pm2)\times10^{-11}$	-13.5±0.2	-12.9±0.2	-0.6±0.3	0.96±0.01
T195A	$1.0(\pm0.4)\times10^{-10}$	-13.4±0.2	-12.9±0.1	-0.5±0.2	0.88±0.01
G196A	$2(\pm3)\times10^{-11}$	-14.2±0.8	-16±1	2±2	1.09±0.03
D197A	$9(\pm3)\times10^{-11}$	-13.5±0.2	-12.2±0.2	-1.3±0.3	1.21±0.02
I280A	$9(\pm2)\times10^{-11}$	-13.5±0.1	-12.6±0.1	-0.9±0.2	1.06±0.01
G281A	$8(\pm3)\times10^{-11}$	-13.6±0.2	-13.1±0.3	-0.5±0.4	0.89±0.01
K283A	$9(\pm2)\times10^{-11}$	-13.5±0.3	-15.3±0.7	1.8±0.2	0.89±0.01

All measurements were performed in 10mM Tris (pH 7.5), 200mM KCl, 2.5mM MgCl$_2$ at 20°C. Each value represents the average of at least two independent ITC titrations. Errors given are 68% confidence intervals propagated from the nonlinear least squares analysis.
[a] Obtained from nonlinear least squares analysis of the titration data to a single site binding model in Origin 7.0.
[b] Measured using direct TAPS titrations, corrected for BirA homodimerization as described in discussion
[c] Entropy, -TΔS°, calculated from titration results using the expression $\Delta G°=\Delta H°-T\Delta S°$
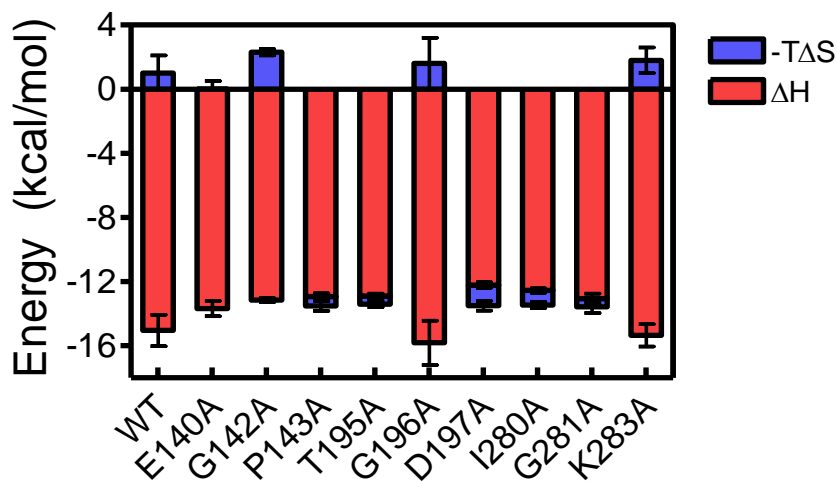
Figure 4.2: Corrected thermodynamic contributions to bio-5'-AMP binding. The enthalpic (red) and entropic (blue) components of the free energy of bio-5'AMP binding for each BirA species studied following correction for BirA homodimerization. Errors bars shown are the propagated 68% confidence intervals.
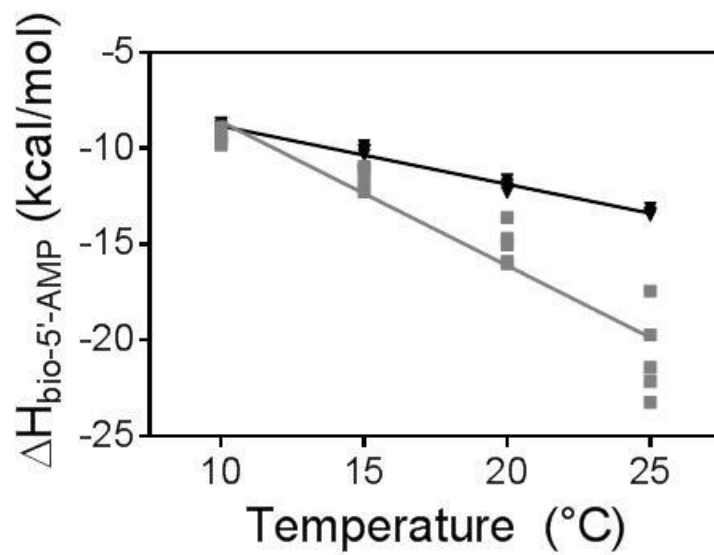
Figure 4.3: Effects of the correction for wild type BirA homodimerization on the heat capacity change of bio-5'-AMP binding.
Data shown are enthalpy of bio-5'-AMP binding as determined by TAPS titrations at 10-25C before (black) and after (grey) applying the correction for BirA homodimerization.

Table 4.3: Corrected heat capacity changes for Bio-5'-AMP binding to BirA variants

Protein	ΔC_P [a] (kcal/mol·K)	$\Delta\Delta C_P$ [b] (kcal/mol·K)
Corrected Wild Type	-0.75±0.06	—
E140A	-0.58±0.05	0.17±0.08
G142A	-0.31±0.01	0.44±0.06
P143A	-0.49±0.02	0.26±0.06
T195A	-0.43±0.02	0.32±0.06
G196A	-0.68±0.06	0.07±0.08
D197A	-0.37±0.01	0.38±0.06
I280A	-0.31±0.01	0.44±0.06
G281A	-0.38±0.01	0.37±0.06
K283A	-0.59±0.04	0.16±0.07

Heat capacity changes of bio-5'-AMP binding to the BirA dimerization surface variants corrected for the presence of BirA dimerization.

[a]Calculated from linear regression of the temperature dependence of the corrected $\Delta H°_{bio\text{-}5'\text{-}AMP}$ (**Figure 3.6**). Uncertainty given in $\Delta C°_p$ is the 68% confidence interval from linear regression.

[b] Change in $\Delta C°_p$ from wild type, $\Delta\Delta C°_p$ Calculated by the expression $\Delta C°_{p,variant} - \Delta C°_{p,wt}$. Uncertainty in $\Delta\Delta C°_p$ is the propagated error in heat capacity change for wild type and BirA variant.
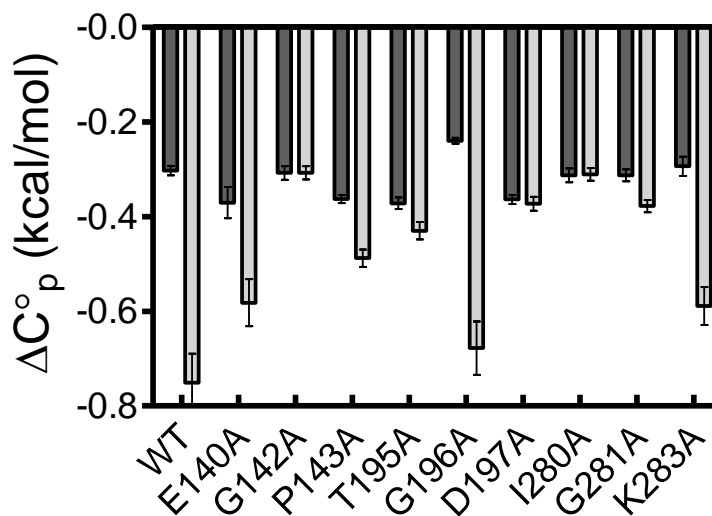
Figure 4.4: Comparison of corrected heat capacity change measurements.
The $\Delta C°_p$ of bio-5'-AMP binding before correction (dark) corrected for the enthalpy of BirA homodimerization (light). Error bars are the standard deviation of the slope from linear regression.
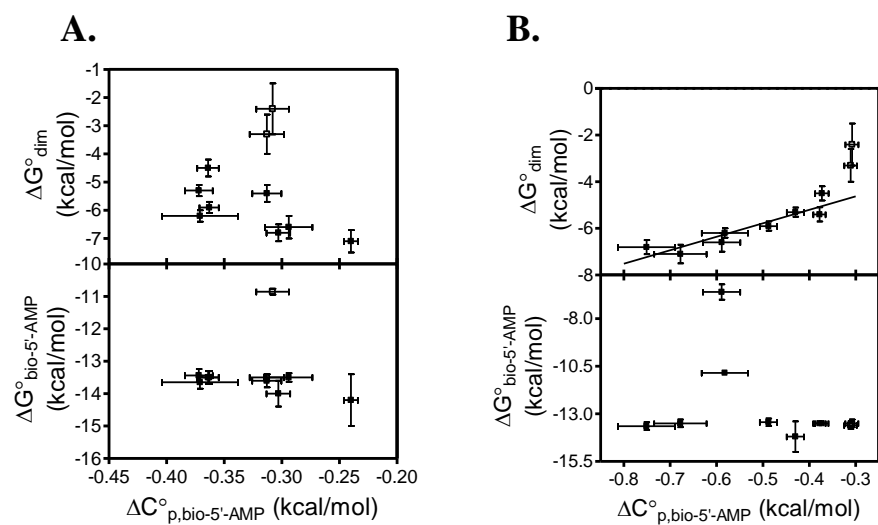
Figure 4.5.Functional correlations of the heat capacity change of bio-5'-AMP binding
The change in heat capacity is illustrated in relation to both dimerization and bio-5'-AMP binding free energies for each BirA variant. Error bars represent the 68% confidence intervals of the respective thermodynamic parameters. A) Correlation plot of the heat capacities as measured. B) Correlation plot using the corrected heat capacity values. BirA variants G142A and I280A (□) are excluded from the linear regression shown.

capacity changes (Figure 4.4). This correction reveals a striking positive correlation between dimerization free energy and $\Delta\Delta C^{\circ}_p$ (**Figure 4.5B**).Excluding variants G142A and I280A, which are not well-described by a linear function, the remaining variants assume a linear relationship with a slope of 4.5 kcal/mol of dimerization free energy per kcal/mol increase in ΔC°_p.

Interpretations of ΔC°_p have often focused on correlations established to changes in solvent accessible surface area[37]. However, this interpretation has not been demonstrated to be consistent in all systems. Changes in hydrogen bonding and electrostatic interactions have also been demonstrated to give rise to negative heat capacity changes[38,39].

An alternative interpretation given by Alan Cooper is that negative heat capacity changes may be an expected consequence for the disorder to order transitions occurring in BirA. He demonstrates this by deriving ΔC°_p using a statistical thermodynamic model in which a network of interacting subunits undergo a cooperative transition[40]. Following this interpretation, it would be expected that the heat capacity change would be more positive in variants that do not undergo as significant of a disorder-to-order transition. Using this interpretation, the most negative heat capacities are consistent with the full disorder-to-order transition observed in wild type BirA including G196A, E140A and K283A. The remaining BirA variants have significantly more positive heat capacity changes consistent with perturbations of loop folding. Because there are no functional effects observed to ligand binding, these perturbations to loop folding can be tied to the 193-197 disorder to order transition. The heat capacity change results also affirm the predictions[32] from

the G142A structure that disorder-to-order loop folding is coupled to allosteric activation of BirA by demonstrating a direct correlation between dimerization free energy and heat capacity change, a parameter associated with both protein folding and disorder-order transitions.

Formation of intramolecular interactions is observed upon allosteric activation

Analysis of the wild type apo and holoBirA structures reveals multiple intramolecular interactions occurring upon helical extension of residues 143-146 and folding of the 193-197 loop (**Table 4.4**). Disruption of these intramolecular interactions formed upon allosteric activation by alanine substitution has moderate effects on the heat capacity change of bio-5'-AMP binding (Figure 4.4). Due to the correlation between $\Delta\Delta G^{\circ}_{DIM}$ and $\Delta\Delta C^{\circ}_{p}$ these variants also have more positive dimerization free energies consistent with perturbed loop folding. However, there are no obvious intramolecular interactions that exist in wild type holoBirA which would be perturbed in I280A BirA, despite its deficit to free energy of dimerization. Because of the pronounced functional effect observed for these variants and their lack of correlation with heat capacity change, the effects that are observed on the dimerization free energy are beyond perturbation to folding of the 193-197 loop.

Table 4.4: Intramolecular interactions formed upon BirA monomer activation

Residues	Interaction	Atomic Distance (Å)
K194-D197	Salt Bridge	3.4
K194b-D197b	Hydrogen bond	3.0
K194b-A198b	Hydrogen bond	3.4
P143b-A146b	Hydrogen bond	2.9
R119-D282	Salt Bridge	4.1
R119-E313	Salt Bridge	3.7
R118-D176	Salt Bridge	3.0
R118-V189b	Hydrogen bond	3.5

Interactions above are those observed are on the dimerization surface (top) and those at conserved R118 and R119 residues in the BBL(bottom). These were determined from comparing wild type apo BirA (1BIA) to the holo (2EWN) structure.

Chapter 5 : Conclusions and Future Directions

The results indicate a model for allosteric activation of the BirA monomer in which bio-5'-AMP binding and folding of the ABL induce an alpha helical extension of residues 143-146. This helical extension optimizes the dimerization surface for formation of intramolecular interactions and subsequent folding of the 193-197 loop. Proper folding and arrangement of these regions occur in activation of the molecule for dimerization. However, the mechanism by which the allosteric signal is communicated to residues 143-146 is not clear from this study.

Because there are no other observable structural consequences in G142A BirA, investigation of this mechanism must proceed by either garnering further structural data of alanine mutations that perturb the alpha helical transition, or by non-structural methods such as molecular dynamics (MD) simulations that investigate the changes of protein dynamics upon BirA activation. Evidence from prior H/D exchange mass spectra[41] indicate a global dampening of BirA dynamics upon allosteric activation, suggesting that investigation of the role of protein motions may be required for full understanding the molecular mechanism of BirA allostery. Analysis of correlated motions and residue-residue contacts[42] using molecular dynamics simulations could provide insight and, more importantly, testable hypotheses to further investigate how the α-helical extension of the 143-146 residues is occurring.

Chapter 6 : Appendicies

Appendix 1: Discrepancy between ΔH_{TAPS} and $\Delta H_{displacement}$ of bio-5'-AMP binding

The purpose of this appendix is to address a discrepancy that is observed when measuring the enthalpy of bio-5'-AMP binding using two different ITC titration methods. The enthalpies measured by the displacement technique are 1-3 kcal/mol more negative than those measured directly by TAPS titrations. The P143A variant has the largest deviation, $3.1\pm.1$ kcal/mol. Displacement titrations for the remaining proteins also yielded more favorable enthalpies by 1-2.5 kcal/mol except for G142A BirA, for which a displacement titration could not be performed (**Figure 6.1**). For this variant, no difference was observed between the direct and TAPS measurement. For this reason and due to the relative simplicity of the direct measurements, investigation into possible sources of the discrepancy was focused on the displacement method. However, a likely source of the more negative enthalpy of binding from displacement titrations was not found. Nontheless, the accuracy of the Gibbs free energies measured by displacement titrations and the enthalpy of bio-5'-AMP binding measured by TAPS titrations are strongly supported by experimental evidence.

Possible sources of experimental discrepancy

To attempt to discern the source of the 1-3 kcal/mol deviation observed between TAPS and displacement-obtained enthalpies of binding, differences in both experimental protocol and reagents used were examined. The enthalpies determined for I280A and K283A BirA by the displacement method were first reproduced using
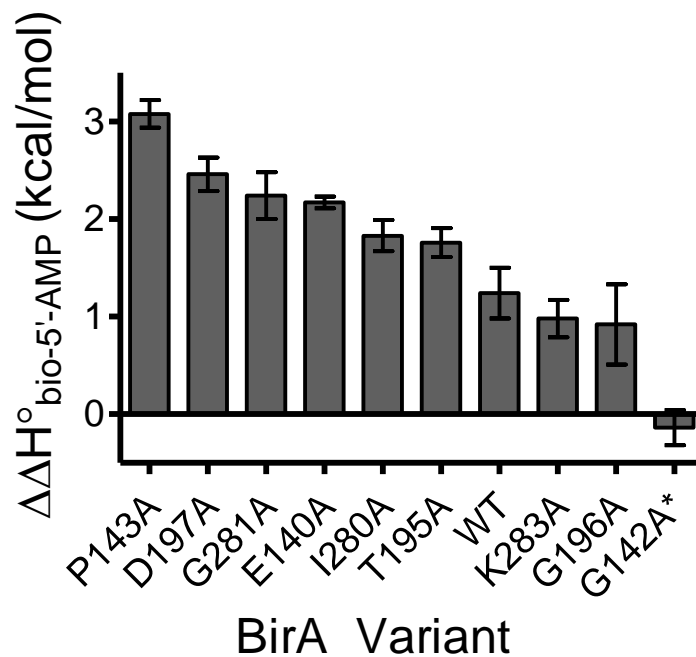
Figure 6.1. Discrepancy between bio-5'-AMP binding enthalpy from TAPS and displacement ITC measurements.
Values of ΔΔH °Calculated by $\Delta\Delta H° = \Delta H°_{TAPS} - \Delta H°_{Disp}$ for each BirA variant. Protein and ligand solutions for both methods were prepared in 10mM Tris (pH=7.50 at 20°C), 200mM KCl, 2.5mM $MgCl_2$. Errors reported are the propagated 68% confidence interval of the individual enthalpy measurements.

new reagents (**Table 3.1Table 6.1**). The deviation was reproducible using different reagents at a later date. Because of this, it is not believed that there is any systematic error due to the reagents used or the order in which experiments were performed. To further demonstrate the ligand was intact for these titrations, the bio-5'-AMP solution was analyzed by TLC (see materials and methods). The presence of contaminating biotin in the bio-5'-AMP reagent was a concern because of its more negative enthalpy of binding. However, the presence of only a single spot at the correct retention distance, 0.53, was indicative of no contaminating biotin in the solution.

Additionally, systematic experimental deviations could stem from differences in the protocol between the two methods. Displacement titrations uniquely require the inclusion of saturating biotin and this presence of excess biotin represents a difference in the chemical environment of the bio-5'-AMP binding reaction. To determine if the excess biotin used affected the enthalpy of corepressor binding, displacement titrations were performed using both 3μM and 6μM biotin for I280A BirA. A $\Delta\Delta H°$ between methods of 1.4±0.1 and 1.6±0.1 kcal/mol, respectively, was still observed at both concentrations. These results indicate that the presence of excess biotin, which was present in each displacement titration, does not significantly affect the measured enthalpy of bio-5'-AMP binding.

Table 6.1. Reproduction of displacement titration measurements

I280A BirA	$K_{D,bio-5'-AMP}$ (M)	$\Delta G^\circ_{bio-5'-AMP}$ (kcal/mol)	$\Delta H^\circ_{bio-5'-AMP}$ (kcal/mol)	$-T\Delta S_{bio-5'-AMP}$ (kcal/mol)	n
Original	$9(\pm1)\times10^{-11}$	-13.5±0.1	-14.5±0.1	1.0±0.1	1.16±0.01
Reproduction	$1.0(\pm0.2)\times10^{-10}$	-13.4±0.2	-14.4±0.1	1.0±0.2	0.97±0.01
K283A BirA					
Original	$1.1(\pm0.2)\times10^{-11}$	-13.4±0.1	-14.8±0.1	1.4±0.1	0.87±0.1
Reproduction	$1.1(\pm0.4)\times10^{-11}$	-13.3±0.2	-15.2±0.2	1.9±0.2	0.87±0.1

Measured at 20°C by displacement ITC titration in 10mM Tris (pH=7.50 at 20°C), 200mM KCl, 2.5mM $MgCl_2$. Each parameter represents the results from non-linear least squares regression of a single ITC isotherm. The uncertainty provided is the 68% confidence interval provided by linear regression.

ΔG°_{bio-5'-AMP} measured by biotin displacement agrees with those measured by direct titrations.

Because of the presence of this discrepancy between the measured enthalpies of bio-5'-AMP, the accuracy of the parameters obtained from both methods were in question. Measurement of the Gibbs free energy and the enthalpy of bio-5'-AMP binding by ITC is inherently coupled, however it was possible to validate the free energy values obtained by direct comparison to the results of a direct titration. To perform this experiment, a variant was carefully chosen so that its c-value would be within the measureable range for both direct and biotin displacement titrations. The BirA variant W223A allowed for these measurements, providing c-values of ~8 and ~300 for the displacement and direct titrations respectively (**Figure 6.2**). These measurements yielded $\Delta G^\circ_{\text{bio-5'-AMP}}$ of -11.7±0.2 -11.2±0.2 indicating that the Gibbs free energies as measured by displacement titrations well-represent those that cannot be determined directly(**Table 6.2**). In additional support of the of the Gibbs free energy values obtained by this method, the wild type $\Delta G^\circ_{\text{bio-5'-AMP}}$ (**Table 3.3**) is within 0.5 kcal/mol of that calculated from the results of previous kinetic measurements, -13.6±0.2 kcal/mol[43]. For this reason it is believed that the free energies obtained by biotin displacement ITC titrations are valid and therefore were not excluded from this study.
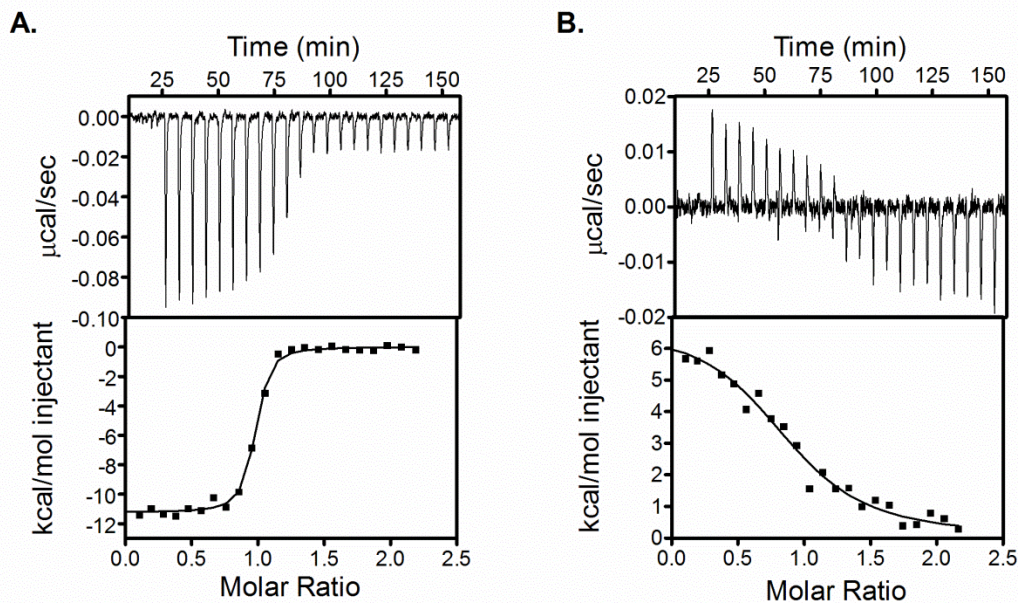
Figure 6.2 Direct versus Displacement titration of W223A BirA.
Data is illustrated for both direct binding(A) and displacement(B) ITC methods. Protein and ligand solutions were prepared in 10mM Tris (pH=7.50 at 20°C), 200mM KCl, and 2.5mM MgCl$_2$. The top panel is the ITC data trace following manual baseline correction. After integration and normalization to the moles of injectant, the binding isotherm, bottom panel, is obtained. Non-linear least squares regression of each isotherm to the single-site binding model provides the ligand binding parameters.

Table 6.2 Comparison of direct and displacement bio-5'-AMP binding measurements.

W223A BirA	$K_{D, bio-5'-AMP}$ (M)	$\Delta G°_{bio-5'-AMP}$[a] (kcal/mol)	$\Delta H°_{bio-5'-AMP}$ (kcal/mol)	$-T\Delta S°_{bio-5'-AMP}$[b] (kcal/mol)	n
Direct Binding	$4(\pm1)\times10^{-9}$	-11.2±0.2	-11.3±0.2	0.1±0.3	0.91±0.01
Biotin Displacement	$1.8(\pm0.5)\times10^{-9}$	-11.7±0.2	-12.5±0.4	0.8±0.4	0.98±0.02

All measurements were performed in 10mM Tris (pH 7.5), 200mM KCl, 2.5mM MgCl2 at 20°C. Each value represents the average of at least two independent ITC titrations. Errors given are 68% confidence intervals propagated from the nonlinear least squares analysis.

ΔH°_{biotin} measured directly agrees with that measured by TAPS titration.

Because of the discrepancy between direct and displacement ITC titrations, it must be determined which method most accurately provides the enthalpy of bio-5'-AMP binding. Ultimately, biotin displacement is an indirect measurement of both the enthalpy and free energy of bio-5'-AMP binding. The parameters determined from this competitive assay have a lower signal-to-noise and rely on accurate measurement of the enthalpy and association constant of biotin, both of which have an associated error. Due to the comparative complexity of the displacement titrations, it is believed that the binding enthalpy obtained from TAPS measurements provides a more accurate value. To demonstrate this, the enthalpies of biotin binding, which have also been characterized by full-direct titrations in this study, were reproduced for three dimerization surface variants using the TAPS method (**Figure 6.3**). No deviation was observed for both K283A BirA and E140A BirA. P143A BirA was also examined in this way and a small deviation, $\Delta\Delta H^\circ = 0.5\pm0.3$ kcal/mol, was measured between TAPS and direct titrations (**Figure 6.4, Table 6.3**). However, this difference is much smaller than that measured between TAPS and displacement methods, 3.1 ± 0.1kcal/mol. These results demonstrate reproducibility and consistency of the enthalpies determined from TAPS measurements compared to those determined from direct titrations. Therefore, the molar enthalpies of bio-5'-AMP binding determined from displacement titrations were not analyzed in this study and instead only those values obtained from TAPS titrations were considered. Ultimately, these enthalpies were used to calculate the entropic components ($-T\Delta S$) and heat capacity changes of bio-5'-AMP binding to the BirA variants.
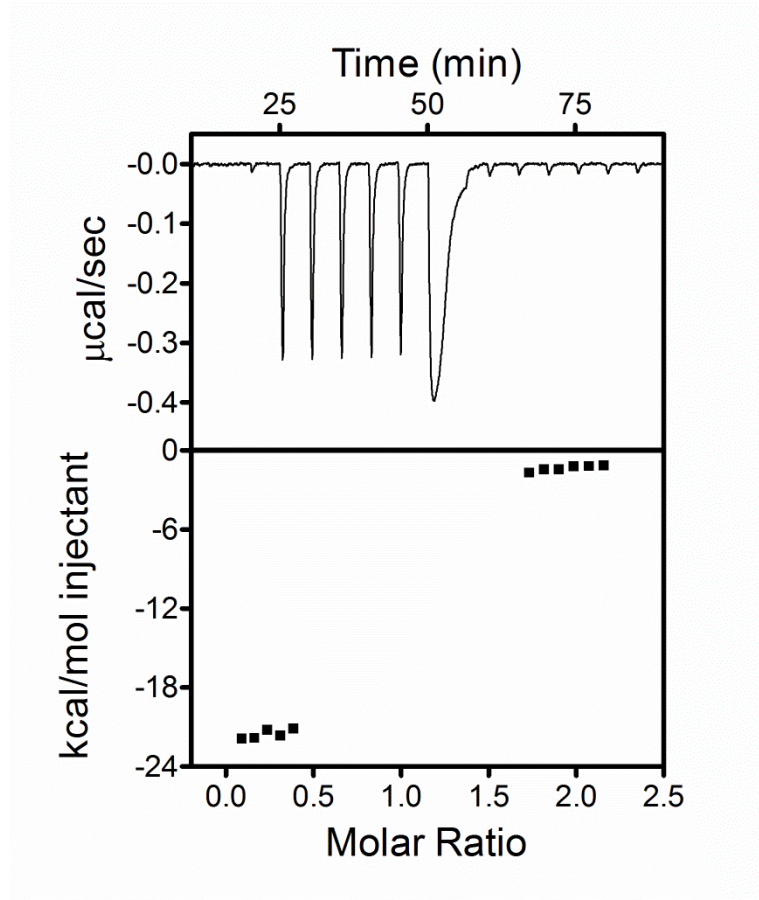
Figure 6.3 Biotin TAPS titration of P143A BirA.
Both protein and ligand solutions were prepared in 10mM Tris (pH=7.50 at 20°C), 200mM KCl, 2.5mM MgCl$_2$. The top panel is the ITC data trace following manual baseline correction. After integration and normalization to the moles of injectant, the binding isotherm, bottom panel, is obtained. The difference between the molar heat before and after protein saturation provides the enthalpy of ligand binding.
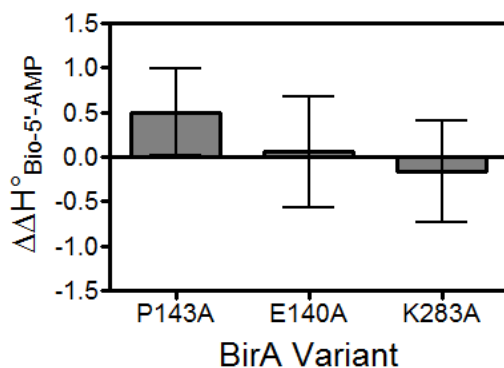
Figure 6.4 Difference of bio-5'-AMP binding enthalpy between direct and TAPS ITC measurements.
Values of ΔΔH °Calculated by ΔΔH°=ΔH°TAPS-ΔH°Direct for each BirA dimerization surface variant. Protein and ligand solutions for both methods were prepared in 10mM Tris (pH=7.50 at 20°C), 200mM KCl, 2.5mM $MgCl_2$.Errors reported are the propagated 68% confidence interval of the individual enthalpy measurements.

Table 6.3 Biotin binding enthalpy obtained from TAPS measurements.

BirA Variant	$\Delta H°_{biotin}$ (kcal/mol)	$\Delta\Delta H°_{biotin}$ (kcal/mol)
P143A	-20.2±0.4	0.5±0.4
E140A	-20.1±0.5	0.0±0.5
K283A	-20.6±0.4	0.2±0.5

Biotin TAPS titrations performed in 10mM Tris (pH=7.50 at 20°C), 200mM KCl, 2.5mM $MgCl_2$
A large protein concentration, 5μM, was used to assure stoichiometric biotin binding. Enthalpies reported from the average of two TAPS titratrations containing five pre-saturation injections each. Errors reported are propagated 68% confidence intervals. $\Delta\Delta H°_{biotin}$ calculated using the equation $\Delta\Delta H°_{biotin}=\Delta H°_{TAPS}-\Delta H°_{Direct}$ where $\Delta H°_{Direct}$ values are those listed in Table 3.2.

Appendix 2:Considerations in the Design of ITC experiments

All ITC titrations in this study were designed with several experimental factors in mind which are detailed below. Particularly, careful consideration was given to the Wiseman 'c' value[44] and the concentration and size of each ligand injection.

Wiseman's c-value for the design of ITC titrations

The 'c' parameter, where $c = K_A \cdot [P] \cdot n$, is a function of the association constant, K_A, total protein concentration, [P], and binding stoichiometry, n, for a single-site binding interaction. Of these parameters, only the protein concentration is modifiable in the design of a simple binding ITC experiment. This choice is limited on the upper and lower bounds by the quantity of protein able to be purified and the minimum protein concentration required to achieve a measureable heat of interaction upon injection (ideally ~5μcal or more, but as low as ~1μcal can be analyzed with quality data). In this study, increasing the protein concentration was also limited by the presence of a coupled homodimerization reaction. Nonetheless, the c-value was maintained within the recommended range of about 5-500, because titration data with a c-value outside this range provide a binding curve with less information about the binding process The titration curve asymptotically approaches a step-function (**Figure 6.5**)., which contains no information regarding the association constant of binding, at large-c-values (stoichiometric binding). However, both the experimental stoichiometry and enthalpy of binding are very well-determined under these
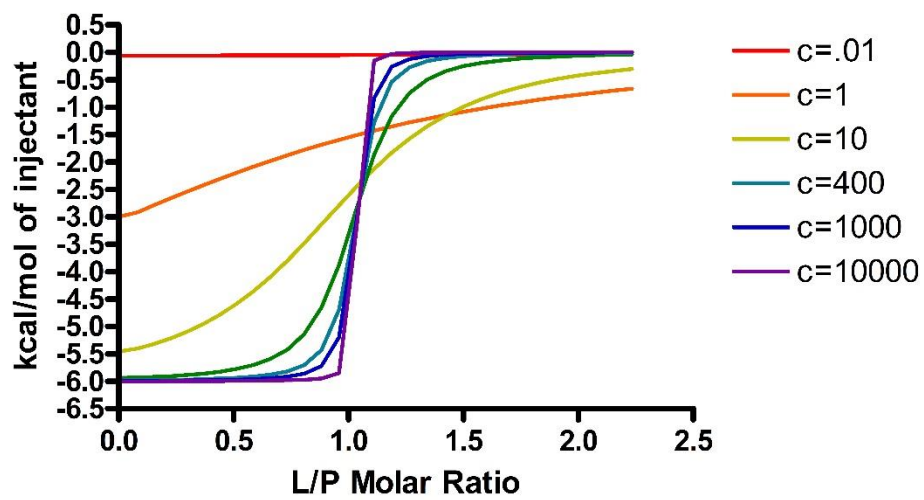
Figure 6.5 Simulated influence of c-value on single-site ITC binding curve.
Heat of injection from c=0.01 to c=1x10^4 were simulated using the parameters: ΔH=-6kcal/mol, K_D=2x10^{-8}M, and n=1. The protein concentration was varied in each case to obtain differing c-values.

conditions, which is the basis of total association at partial saturation (TAPS) measurements. Values obtained from small c-value binding curves can be misleading, because they generally do not reach saturation over the course of titration. Therefore, these measurements provide only a small portion of the full binding curve from which an accurate stoichiometry and enthalpy of binding cannot be determined. The association constant of binding is theoretically accessible at a low c-value (as long as the heats of binding upon injection are measureable), but precautions must be taken to assure full protein saturation[45]. C-values utilized were approximately 100 and 100,000 for the direct biotin binding and bio-5'-AMP TAPS measurements, respectively.

Although the c-value is a parameter derived from the single-site binding equation, it can also be used to describe the biotin displacement titrations in this study. This is because the competition titrations performed were all using saturating concentrations of the competing ligand, which results in a pseudo-single-site binding curve for which the apparent association constant is a function of the K_A of both ligands and the concentration of competing ligand as shown below:

$$K_{app} = \frac{K_{A,bio5'AMP}}{1 + K_{A,biotin}[biotin]}$$

Therefore the c-value of a displacement titration is calculated using the *apparent* association constant. Decoupling of the actual binding constant from the c-value is what permits competitive binding assays to measure association constants significantly tighter than those accessible by only direct binding. A typical c-value obtained for these displacement titrations was ~250.

58

Ligand concentration and injection scheme

Another important consideration in the design of ITC titrations is determining the quantity of ligand to be injected and the number of injections over which this will occur. The quantity of ligand injected should be large enough that the protein is ultimately saturated with ligand at the end of the titration. Unless the c-value of the titration is particularly low, a final ligand/protein ratio of 2.2-2.5 is acceptable for complete saturation. This translates to a ligand concentration about 10-fold larger in the injection syringe than the protein concentration present in the sample cell. Titration with a quantity of ligand much greater than this will than this will, because the protein is saturated after only several injections, only provide a fraction of the binding curve. Determination of the stoichiometry and enthalpy of binding will then be difficult (**Figure 6.6**).

In the determination of an injection scheme, or what quantity and size of ligand injections to use, the use of a simulation program is highly recommended. To maximize the amount of data available for nonlinear-least squares regression, a full, symmetrical binding curve, with several injections before and after protein saturation, should be used (see **Figures 3.1, 3.3** for examples**)**. For this study, the titration parameters were optimized by simulating ITC titrations using a spreadsheet provided by T. Biswas and O.V. Tsodikov[29] (**Figure 6.7**). Injection volumes were chosen so that multiple injections (3-4) were present on the saturation and pre-saturation binding plateaus.
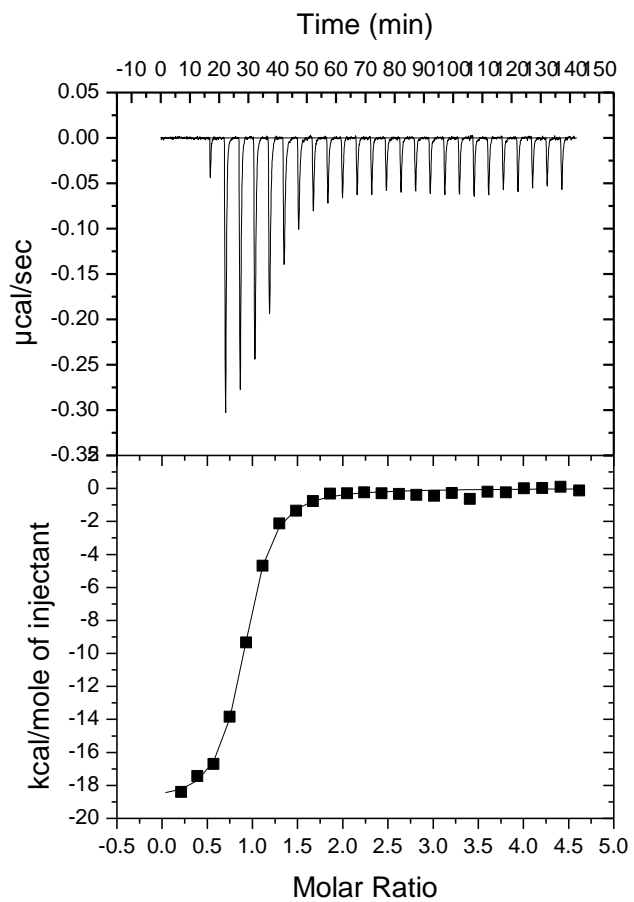
Figure 6.6 Example ITC titration using excess ligand.
Too much ligand was used, resulting in early saturation of the protein in the course of this direct biotin titration.

	A	B	C	D	E	F	
1		cell volume, µL	[syringe concentration of L], µM	[cell species, P]init in µM	injection #	injection volume, µL	[L
2		1440	20	2	1	2	
3					2	13	
4					3	13	
5					4	13	
6	Kd, µM		ΔH (kcal/mole of complex formed)		5	13	
7	0.02		-20		6	13	
8			100		7	13	
9					8	13	
10			ΔH (cal/M of complex formed)		9	13	
11			-28.8		10	13	
12					11	13	
13	See last column for heat values				12	13	
14					13	13	
15					14	13	
16					15	13	
17					16	13	
18					17	13	
19					18	13	
20					19	13	
21					20	13	
22					21	13	
23					22	13	
32					total volume=	275	
33						To add injections,	
34						continue the volumes, then extend do	
37						Citation: Biswas, T. and Tsodikov, O.V. (2010)	

Figure 6.7 Simulation of a direct biotin binding titration.

This Microsoft-Excel-based tool allows simulation of single-site and pseudo single-site binding titrations. The user provides the experimental parameters (green, yellow, or grey cells) and the heat of injection is calculated for an indicated number of injections u sing the single-site binding model.

Appendix 3: Expression and purification of BirA variants

BirA alanine variants used in this study were expressed and purified as previously described[18,20], except for variants E140A and K283A which were prepared as follows. Approximately 50ng of pBtac2 BirA-(His$_6$) plasmid[25] DNA containing the appropriate variant coding sequence was transformed at 1500V into 50μL of JM109 electrocompetent cells. Immediately after electroporation (BTX-ECM399), cells were suspended in 1mL of cold SOC media and incubated at 37°C for an hour. Both 5μL and 20μL of transformed cells were spread evenly onto separate LB/AMP agar plates and subsequently grown at 37°C overnight. The pBtac2 BirA-(His$_6$) plasmid contains the β-lactamase gene that confers ampicillin resistance. Inclusion of ampicillin (100μg/mL) in both LB agar and the liquid media allowed for selection of only transformed colonies.

Following transformation, 2-3 well-separated colonies were inoculated into 5mL of LB/AMP and shaken overnight at 37°C. Prior to their usage for the large-scale preparation of BirA, the induction of each cell line was assessed by a small-scale induction trial. To perform this trial, half of each overnight culture (2.5mL) was inoculated into 20mL of sterile LB/AMP. The remaining 2.5mL of culture was stored at 4°C until needed. After inoculation, the 20mL culture was incubated at 30°C until the OD$_{600}$ reached 0.6. At this point, 0.5mL aliquots of each culture were removed as a pre-induction sample. These samples were pelleted by centrifugation for 5 minutes at 10,000rpm and stored at -20°C for subsequent SDS-PAGE analysis. Because the pBtac2 BirA-(His$_6$) plasmid is transcriptionally controlled by the tac promoter, overexpression of BirA variants was induced by addition of IPTG to 1mM final

concentration. After 4 hours of 200 rpm shaking at 30°C, the OD_{600} of each culture

was recorded and a second 0.5mL aliquot was removed from each induction trial for

analysis. These aliquots were similarly pelleted as above, and all cell-pellets were

decanted then dissolved in a volume, $\frac{OD_{600}}{12}$ mL, of Laemmeli sample buffer[26] (LSB)

normalized to the OD_{600} of the culture at the time it was removed. This process

confers a constant protein concentration to all SDS-PAGE samples so they may be

qualitatively compared. The culture that demonstrated the highest induction of BirA,

and of no other proteins, was chosen for large-scale protein preparation. The

remaining 2.5mL of the chosen cell line was inoculated into 300mL of LB/AMP and

shaken (200rpm) overnight at 37°C as a starter culture for protein expression.

The 300mL overnight culture was evenly divided into two 4L Erlenmeyer

flasks, each containing 2L of sterile LB/AMP media. Cells were grown at the

induction temperature, 30°C, with shaking at 175rpm until the OD_{600} reached

approximately 0.8. At this point, a 0.5mL aliquot was removed and pelleted as above

for SDS-PAGE analysis. Overexpression was induced by adding IPTG to a final

concentration of 1mM. After starting induction, the cultures were shaken for an

additional 4 hours in identical conditions. Once induction was complete, the cell

solutions were cooled on ice to 4°C. Care was taken to keep the cell solutions, cell

pellet, and cell lysate at this temperature throughout the preparation steps to preserve

BirA integrity. A 1L centrifugation bottle (Hitachi) was weighed prior to pelleting the

cells, so that total cell mass could later be determined. The cell suspension was

pelleted by centrifugation 2L at a time at 4500 rpm for 20 minutes at 4°C. This

centrifugation (Sorvall RC 5B Plus) step was performed by dividing the cell

suspension evenly (about 500mL x4 bottles) and carefully balancing (±0.5g) the suspension between bottles placed oppositely into the F8S-4x1000y rotor. The cell pellets were then washed by suspension in excess lysis buffer (50mM NaH_2PO_4, 300mM NaCl, 10mM Imidazole, 5% glycerol, 100μM DTT, pH 8), and combined into a single pre-weighed centrifuge bottle. After a second centrifugation at 4500rpm for 20 minutes, the lysis buffer was carefully decanted and the mass of the remaining cell pellet weighed on an analytical balance. Cells were gently suspended by Pasteur or transfer pipet into 5mL of lysis buffer per gram of cell pellet.

For lysis, the cells were transferred to the smallest-allowable, pre-chilled metal lysis cup. The sample was sonicated (Branson Sonifier 450) for 2-minute intervals in lysis buffer at sonifier output and duty cycle of 60% to minimize sample heating. The cell lysate was maintained below 10°C during lysis using a salt/ice bath. To inhibit serine protease activity, 0.01% of the total cell lysate volume of 100mM PMSF was introduced prior to each sonication interval. Lysis was considered complete when the OD_{600} of a cell lysate sample (diluted 1:100 in lysis buffer) was <10% of the initial value. Centrifugation at 5.4 x g for 30min at 4°C was performed to remove cell debris. Nucleic acids were precipitated from the decanted supernatant by adding PEI (pH=7.5) to a final concentration of .1% (v/v) at 4°C for at least 15 minutes. Another centrifugation step at 5.4 x g for 30min at 4°C pelleted the resulting PEI precipitate. Both cell debris and PEI pellet were suspended into lysis buffer in a volume equal to the respective supernatant. Aliquots (0.5mL) of both precipitate suspensions and both supernatants were removed for SDS-PAGE analysis. Before continuing with protein purification, both overexpression of BirA and its

presence in the PEI supernatant was confirmed by a 12.5% SDS-PAGE gel. The sample from each expression and purification step was diluted 1:1 into LSB, mixed well and heated at 90°C prior to loading 10uL onto a 12.5% acrylamide SDS-PAGE gel, prepared according to the Laemmli discontinuous gel system[26].

Purification of BirA variants from the resulting crude lysate was performed by several chromatography steps using an ÄKTA Prime (GE) liquid chromatography system. All resins were packed in a 1.5cm diameter Bio-Rad econo-column. Between 4 and 5cm (about 7mL) of resin was packed in each 15cm column. Each resin used for purification, except the HA Ultrogel, was regenerated before purification using a resin-specific protocol (see resin regeneration). All resins were equilibrated with at least 10 column volumes of resin-specific starting buffer directly before use. Because the variants have a C-terminal His_6-tag, a nickel affinity column (Ni-NTA agarose, Qiagen) was the first BirA purification step. After dialysis of the PEI supernatant into fresh lysis buffer (at least 2 L, twice), the protein solution (about 150mL) was loaded at 1mL/min onto 7mL of Ni-NTA resin. BirA was eluted in 5mL fractions using an imidazole step gradient starting from 20mM, and proceeding to 50mM, 100mM and finally 250mM. This gradient was performed by eluting with 0%, 13%, 34%, and 100%, respectively, of elution buffer in Ni-NTA starting buffer (50mM NaH_2PO_4, 300mM NaCl, 20mM imidazole, 100μM DTT, 5% glycerol, pH=8) at 0.5mL/min. Each elution step was begun only after the A_{280} was constant for at least 5 minutes. The E140A variant and K283 variant eluted at 50mM and 100mM imidazole, respectively. Following SDS-PAGE (12.5%) analysis of each fraction (1:1 in LSB), those that indicated significant purification of BirA as compared to a 5μL pre-column

sample were pooled and exchanged twice by dialysis against 2L (about 25:1 buffer:dialysate) of SP-sepharose starting buffer.

The second purification step for both E140A and K283A was chromatography on SP-sepharose (GE-Healthcare) cation exchange resin. After equilibration of 7mL of resin with SP-sepharose starting buffer (50mM Tris pH 7.5 at 4°C, 50mM KCl, 100mM DTT, 5% glycerol), the protein solution was loaded at 0.9mL/min. The BirA variants were eluted using a linear KCl gradient from 0.05M-0.8M (0-100% elution buffer) over 110mL. BirA elution was observed at about 0.3M KCl (33% elution buffer) for both variants.

Additional purification of the E140A BirA variant was performed using a Q-sepharose (GE-Healthcare) anion exchange resin using the same loading, elution, and regeneration steps as the SP resin, except that the resin was stored in only 20% ethanol. BirA is eluted at a low salt concentration from the Q-sepharose column, for some mutants this occurs in the wash step. Consequently, 2mL fractions were taken during loading and starting buffer wash in addition to the elution gradient.

Following two 500mL (33:1) dialysis steps of the 15mL protein solution into HA starting buffer, further purification of the E140A BirA variant was achieved using a hydroxyapatite Ultrogel (Pall) mixed-mode resin. The protein solution was loaded at 0.5mL/min onto 5mL of HA resin equilibrated in starting buffer. The protein was eluted at 0.5mL/min using a linear 0.05M-0.5M phosphate gradient, or 0-100% HA elution buffer (50mM sodium phosphate pH=6.5, 100μM DTT, 5% glycerol) in HA starting buffer over 100mL. Each 3mL fraction containing pure E140A BirA, according to 12.5% SDS-PAGE gel analysis, was pooled and dialyzed in 1L (37:1)

of storage buffer (200mM KCl, 50mM Tris, 100µM DTT, 5% glycerol, pH=7.5 at 4°C).

All purified variants were dialyzed twice in at least 1:30 of protein:storage buffer and filtered using a 0.22um PVDF syringe filter pre-rinsed in storage buffer. The final protein solutions were mixed carefully to achieve homogeneity and aliquoted into 1mL fractions for storage at -80°C. Coomassie brilliant blue stains of samples subjected to 12.5% SDS-PAGE indicated that all BirA variants were ≥95% pure. Stoichiometric bio-5'-AMP binding titrations, monitored by fluorescence spectroscopy, indicate ≥85% ligand binding activity. BirA concentration was determined by the average of three measurements of the absorbance at 280nm using the molar extinction coefficient, 47510 $M^{-1}cm^{-1}$, calculated from the protein sequence[27]. Each measurement of concentration was a different BirA dilution prepared gravimetrically in storage buffer to obtain a range of A_{280} between 0.2 and 0.8.

Preparation and regeneration of FPLC chromatography resins

After use, each resin was regenerated as described below. Additionally, all resins that had been previously used were regenerated prior to protein purification. To avoid cross-contamination between protein solutions, a single resin aliquot was used to prepare only one specific BirA variant. In contrast to the other resins, the hydroxyapatite (HA) Ultrogel (PALL) was only regenerated after use since it was newly obtained. All resins were cleaned at 4°C by gravity-flow of a series of reagents. Each reagent was allowed to reach the column bed before the next was introduced.

Regeneration and storage of the Ni-NTA resin following purification was performed with slight modification from the manufacturer's recommendation (QIAGEN). First 1 column volume (c.v.) of Ni-NTA elution buffer (50mM sodium phosphate pH=8, 300mM NaCl, 250mM imidazole, 100μM DTT, 5% glycerol,) followed by 2 c.v. of Ni-NTA regeneration buffer (6M guanidinium hydrochloride, 0.2M acetic acid) were flowed through the resin. It was then equilibrated with 5 c.v. of MQH$_2$O followed by 3 c.v. of 2% sodium dodecyl sulfate (SDS) in water. Subsequently, 1 c.v. of first 25%, then 50%, and finally 75% ethanol was used. The column was then washed with 5 c.v. of 95% ethanol, then again with 1 c.v. of 75%, 50%, and finally 25% ethanol. After a 1 c.v. rinse with MQH$_2$O, the column was equilibrated in 5 c.v. of 100mM ethylenediaminetetraacetic acid (EDTA). This step removes chelated nickel (II), so the resin should lose its blue color. Following a 5 c.v. MQH$_2$O wash to remove any EDTA present, the nickel is restored by rinsing the resin with 2 c.v. of 100mM NiSO$_4$ in water. A 2 c.v. regeneration buffer rinse was used afterwards to remove excess nickel (II). If significant color does not remain, new resin is required. The resin is then equilibrated in 5 c.v. lysis buffer (50mM NaH$_2$PO$_4$, 300mM NaCl, 10mM Imidazole, 5% glycerol, 100μM dithiothreitol (DTT), pH 8), at which point it was used for protein purification. For storage after regeneration, the resin was equilibrated in 5 c.v. of 30% ethanol at 4°C.

Regeneration of the SP-sepharose column was performed by gravity-flow of 2 c.v. of 2M NaCl, followed by 10 c.v. of 1M NaOH, and finally 8 c.v. of 70% ethanol. The regenerated resin was equilibrated with 5 c.v. of SP-sepharose starting buffer (50mM Tris, 50mM KCl, 100μM DTT, 5% glycerol, pH=7.5 at 4°C) for protein

purification, or in 20% ethanol, 0.2M sodium acetate for storage at 4°C. The Q-sepharose column was regenerated and stored identically, except that it was stored without sodium acetate.

The HA resin was regenerated by gravity flow of 4 c.v. of 500mM sodium phosphate pH=6.8, followed by 4 c.v. of 0.1M NaOH, and another 4 c.v. of 500mM sodium phosphate pH=6.8. Prior to storage, the resin was equilibrated in 5 c.v. of HA starting buffer (50mM sodium phosphate pH=6.5, 100μM DTT, 5% glycerol) containing 0.04% sodium azide to inhibit bacterial growth.

Bibliography

1.   Nussinov, R. & Tsai, C.-J. Allostery in Disease and in Drug Discovery. *Cell* **153,** 293–305 (2013).

2.   Johnson, L. N. Glycogen phosphorylase: control by phosphorylation and allosteric effectors. *FASEB J.* **6,** 2274–2282 (1992).

3.   Macol, C. P., Tsuruta, H., Stec, B. & Kantrowitz, E. R. Direct structural evidence for a concerted allosteric transition in Escherichia coli aspartate transcarbamoylase. *Nat. Struct. Mol. Biol.* **8,** 423–426 (2001).

4.   Daly, T. J. & Matthews, K. S. Allosteric regulation of inducer and operator binding to the lactose repressor. *Biochemistry* **25,** 5479–5484 (1986).

5.   Ferreon, A. C. M., Ferreon, J. C., Wright, P. E. & Deniz, A. A. Modulation of allostery by protein intrinsic disorder. *Nature* **498,** 390–394 (2013).

6.   Monod, J., Wyman, J. & Changeux, J.-P. On the nature of allosteric transitions: A plausible model. *J. Mol. Biol.* **12,** 88–118 (1965).

7.   Koshland, D. E., Némethy, G. & Filmer, D. Comparison of Experimental Binding Data and Theoretical Models in Proteins Containing Subunits*. *Biochemisty* **5,** 365–385 (1966).

8.   Perutz, M. F. Stereochemistry of Cooperative Effects in Haemoglobin: Haem–Haem Interaction and the Problem of Allostery. *Nature* **228,** 726–734 (1970).

9.   Datta, D., Scheer, J. M., Romanowski, M. J. & Wells, J. A. An Allosteric Circuit in Caspase-1. *J. Mol. Biol.* **381,** 1157–1167 (2008).

10. Zhang, J. & Matthews, C. R. Ligand Binding Is the Principal Determinant of Stability for the p21H-ras Protein. *Biochemistry* **37,** 14881–14890 (1998).

11. Uversky, V. N. A Protein-Chameleon: Conformational Plasticity of α-Synuclein, a Disordered Protein Involved in Neurodegenerative Disorders. *J. Biomol. Struct. Dyn.* **21,** 211–234 (2003).

12. Schmitz, M. L. *et al.* Structural and functional analysis of the NF-kappa B p65 C terminus. An acidic and modular transactivation domain with the potential to adopt an alpha-helical conformation. *J. Biol. Chem.* **269,** 25613–25620 (1994).

13. Oldfield, C. J. *et al.* Flexible nets: disorder and induced fit in the associations of p53 and 14-3-3 with their partners. *BMC Genomics* **9,** S1 (2008).

14. Ward, J. J., Sodhi, J. S., McGuffin, L. J., Buxton, B. F. & Jones, D. T. Prediction and Functional Analysis of Native Disorder in Proteins from the Three Kingdoms of Life. *J. Mol. Biol.* **337,** 635–645 (2004).

15. Zhao, H. & Beckett, D. Kinetic Partitioning Between Alternative Protein–Protein Interactions Controls a Transcriptional Switch. *J. Mol. Biol.* **380,** 223–236 (2008).

16. Streaker, E. D., Gupta, A. & Beckett, D. The Biotin Repressor: Thermodynamic Coupling of Corepressor Binding, Protein Assembly, and Sequence-Specific DNA Binding†. *Biochemistry* **41,** 14263–14271 (2002).

17. Streaker, E. D. & Beckett, D. Coupling of Protein Assembly and DNA Binding: Biotin Repressor Dimerization Precedes Biotin Operator Binding. *J. Mol. Biol.* **325,** 937–948 (2003).

18.   Naganathan, S. & Beckett, D. Nucleation of an Allosteric Response via Ligand-induced Loop Folding. *J. Mol. Biol.* **373,** 96–111 (2007).

19.   Eginton, C., Naganathan, S. & Beckett, D. Sequence–function relationships in folding upon binding. *Protein Sci.* **24,** 200–211 (2015).

20.   Adikaram, P. R. & Beckett, D. Functional Versatility of a Single Protein Surface in Two Protein:Protein Interactions. *J. Mol. Biol.* **419,** 223–233 (2012).

21.   Bains, G. & Freire, E. Calorimetric determination of cooperative interactions in high affinity binding processes. *Anal. Biochem.* **192,** 203–206 (1991).

22.   *The Merck Index*. (Merck & Co., Inc, 1960).

23.   Abbott, J. & Beckett, D. Cooperative binding of the Escherichia coli repressor of biotin biosynthesis to the biotin operator sequence. *Biochemistry* **32,** 9649–9656 (1993).

24.   Lane, M. D., Rominger, K. L., Young, D. L. & Lynen, F. The Enzymatic Synthesis of Holotranscarboxylase from Apotranscarboxylase and (+)-Biotin II. Investigation of the Reaction Mechanism. *J. Biol. Chem.* **239,** 2865–2871 (1964).

25.   Kwon, K., Streaker, E. D., Ruparelia, S. & Beckett, D. Multiple disordered loops function in corepressor-induced dimerization of the biotin repressor. *J. Mol. Biol.* **304,** 821–833 (2000).

26.   Laemmli, U. K. Cleavage of Structural Proteins during the Assembly of the Head of Bacteriophage T4. *Nature* **227,** 680–685 (1970).

27.   Gill, S. C. & von Hippel, P. H. Calculation of protein extinction coefficients from amino acid sequence data. *Anal. Biochem.* **182,** 319–326 (1989).

28.   *VP-ITC MicroCalorimeter User's Manual*. (MicroCal, LLC).

29.   Biswas, T. & Tsodikov, O. V. An easy-to-use tool for planning and modeling a calorimetric titration. *Anal. Biochem.* **406,** 91–93 (2010).

30.   Brown, P. H. & Beckett, D. Use of Binding Enthalpy To Drive an Allosteric Transition. *Biochemistry* **44,** 3112–3121 (2005).

31.   Zhao, H., Streaker, E., Pan, W. & Beckett, D. Protein−Protein Interactions Dominate the Assembly Thermodynamics of a Transcription Repression Complex†. *Biochemistry* **46,** 13667–13676 (2007).

32.   Eginton, C., Cressman, W. J., Bachas, S., Wade, H. & Beckett, D. Allosteric Coupling via Distant Disorder-to-Order Transitions. *J. Mol. Biol.* **427,** 1695–1704 (2015).

33.   Sigurskjold, B. W. Exact Analysis of Competition Ligand Binding by Displacement Isothermal Titration Calorimetry. *Anal. Biochem.* **277,** 260–266 (2000).

34.   Eginton, C. & Beckett, D. A Large Solvent Isotope Effect on Protein Association Thermodynamics. *Biochemistry* **52,** 6595–6600 (2013).

35.   Breiten, B. *et al.* Water Networks Contribute to Enthalpy/Entropy Compensation in Protein–Ligand Binding. *J. Am. Chem. Soc.* **135,** 15579–15584 (2013).

36.   Ferrante, A. & Gorski, J. Enthalpy–Entropy Compensation and Cooperativity as Thermodynamic Epiphenomena of Structural Flexibility in Ligand–Receptor Interactions. *J. Mol. Biol.* **417,** 454–467 (2012).

37.   Loladze, V. V., Ermolenko, D. N. & Makhatadze, G. I. Heat capacity changes upon burial of polar and nonpolar groups in proteins. *Protein Sci. Publ. Protein Soc.* **10,** 1343–1352 (2001).

38.   Jung, H.-I., Bowden, S. J., Cooper, A. & Perham, R. N. Thermodynamic analysis of the binding of component enzymes in the assembly of the pyruvate dehydrogenase multienzyme complex of Bacillus stearothermophilus. *Protein Sci.* **11,** 1091–1100 (2002).

39.   Krogsgaard, M. *et al.* Evidence that Structural Rearrangements and/or Flexibility during TCR Binding Can Contribute to T Cell Activation. *Mol. Cell* **12,** 1367–1378 (2003).

40.   Cooper, A., Johnson, C. M., Lakey, J. H. & Nöllmann, M. Heat does not come in different colours: entropy–enthalpy compensation, free energy windows, quantum confinement, pressure perturbation calorimetry, solvation and the multiple causes of heat capacity effects in biomolecular interactions. *Biophys. Chem.* **93,** 215–230 (2001).

41.   Laine, O., Streaker, E. D., Nabavi, M., Fenselau, C. C. & Beckett, D. Allosteric signaling in the biotin repressor occurs via local folding coupled to global dampening of protein dynamics. *J. Mol. Biol.* **381,** 89–101 (2008).

42.   Johnson, Q. R., Lindsay, R. J., Nellas, R. B., Fernandez, E. J. & Shen, T. Mapping Allostery through Computational Glycine Scanning and Correlation Analysis of Residue–Residue Contacts. *Biochemistry* **54,** 1534–1541 (2015).

43.   Xu, Y. & Beckett, D. Kinetics of Biotinyl-5'-adenylate Synthesis Catalyzed by the Escherichia coli Repressor of Biotin Biosynthesis and the Stability of the Enzyme-Product Complex. *Biochemistry* **33,** 7354–7360 (1994).

44.   Wiseman, T., Williston, S., Brandts, J. F. & Lin, L.-N. Rapid measurement of binding constants and heats of binding using a new titration calorimeter. *Anal. Biochem.* **179,** 131–137 (1989).

45.   Turnbull, W. B. & Daranas, A. H. On the Value of c: Can Low Affinity Systems Be Studied by Isothermal Titration Calorimetry? *J. Am. Chem. Soc.* **125,** 14859–14866 (2003).